Universitat Politècnica de Catalunya
Màster en Métodes Numérics per a l'Enginyeria

Departament de Matemàtica Aplicada III

Numerical modeling of Fluid-Structure Interaction: Coupling between FEM and the response-function-based methodology

by

Jordi Rubio González

Master Thesis

Advisor: Pedro Díez
Serguei Iakovlev

Barcelona, 1st of July

Abstract

In this Thesis we face the creation of a new methodology to modeling the Fluid-Structure Interaction for submerged solids subjected to a shockwave. In this work we introduce a new hybrid analytical-numerical approach combining response-functions-based ideology for modeling the fluid and a Finite Element Method for modeling the solid.

Although the outer shape of the solid has to be circular, within the framework of the response function based method we have been able to develop a methodology for dealing with any inner configuration, both in geometry and materials. This kind of problems are of considerable industrial interest, because they represent a wide range of application both in naval architecture (submarines), subsea pipeline engineering and in general off-shore engineering.

With this new methodology we can provide accurate solutions for simple geometries with far less computational cost than with regular FSI methodologies, enabling a much faster pre-dimensioning of the solution for then being computed with regular FSI methodologies or for creating benchmarks for comparing other methodologies.

Contents

List of Figures

Chapter 1

Introduction

1.1 Motivation of the Problem

Nowadays behavior of underwater structures under an explosion are one the major concerns during their design for a wide range of applications. It is a major concern for instance in some especial cases in naval engineering (submarines are the main example in this field) for evident reasons but also to ensure the resistance of strategic pipelines like oil and gas pipelines off-shore structures in case of an accident or even modern submarine communication cables.

All this structures have as common treat that they can be simplified by an outer cylindrical shape. Nowadays full FSI studies using regular methods like FEM need a lot of computational time making them slow and inefficient in early stages of design. These methods also need a bench of validation tests while developed in order to ensure its accuracy.

So the present work borns as way to enable classic pseudo-analytic methods using Fourier decomposition to couple with more modern FEM methods for the solid. This combination should bring best of the two worlds together (but also some of their limitations) allowing a much lower computational cost and therefore doing the pre-dimensioning much faster and agile.

The proposed method should provide accurate enough solutions so that they can be used as reference solutions for validation cases.

(a) Windmill Farm

(b) Submarine

(c) Off-shore structure

(d) Subsea pipeline

Figure 1.1: Examples of applications

1.2 Goals and Layout

The goals of the present work are:

- Couple Pseudo-Analytic fluid models with FEM solid modes
- Validate the results obtained with classic methods based on Reissner-Mindlin theory.
- Compute more complex geometries and analyze the results
- Import more complex geometries from commercial pre-processor
- Post-proccess results in order to obtain stresses

1.3 Problem description

We are going to solve the effect of a shockwave inside an inviscid fluid, linearly compressible fluid affecting a plane stress/plane strain solid modeled with linear elasticity and small deformations. The only limitation in the solid model is that the outer shape must be circular.

Figure 1.2 represents the scheme of the problem to be solved with all the input parameters, and system coordinates.

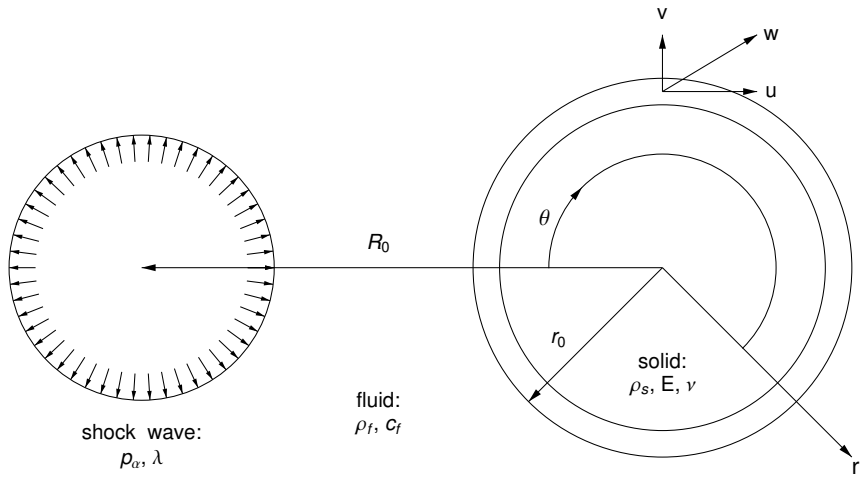

Figure 1.2: Problem Definition

Chapter 2

Modelling the Fluid

2.1 Hypothesis

In the present work some simplifications about the fluid behavior have been done. In particular the fluid has been supposed to be linearly compressible so that the variations in the fluid volume are directly proportional to the variations in pressure. This fact links to the second assumption that has been made. The shockwave does not produce cavitation. Although cavitation is a major engineering concern in the field when produced. This model does not take into consideration effects induced by cavitation, so when very low pressures are observed other methodologies should be used in order to take into consideration this effect.

The fluid has also supposed to be inviscid, so that no energy dissipation is made. This means that the energy condensed in the shock-wave fronts remains constant in time, and that no dissipation is carried in the fluid. Another assumption related to the lack of dissipation is that all properties and formulations are supposed to be independent of the temperature.

The fluid is also supposed to be irrotational. This means that do not exist any discontinuity due to the vortices, and therefore we can write the velocity field as the gradient of a potential function.

The showcase appearing in the fluid is supposed to be cylindrical (circular in the 2D simplification), following a step-exponential law with decay λ.

2.2 Mathematical Formulation

Under the previous considerations we can write the wave equation governing the fluid as:

$$\nabla^2\phi = \frac{1}{c_f^2}\frac{\partial^2\phi}{\partial t^2} \tag{2.1}$$

So it can be re-written in adimensional formulation as:

$$\nabla^2\hat{\phi} = \frac{\partial^2\hat{\phi}}{\partial \hat{t}^2} \tag{2.2}$$

The total pressure at any point can be written as the combination of 3 components. The component due to the incident wave, the component due to the diffracted wave and the component due to the radiated wave, p_0, p_d and p_r respectively.

$$p = p_0 + p_d + p_r \tag{2.3}$$

In adimensional formulation:

$$\hat{p} = \hat{p}_0 + \hat{p}_d + \hat{p}_r \tag{2.4}$$

And the total fluid potential can be written in the same way.

$$\phi = \phi_0 + \phi_d + \phi_r \tag{2.5}$$

And once more we can write down the expression in adimensional formulation

$$\hat{\phi} = \hat{\phi}_0 + \hat{\phi}_d + \hat{\phi}_r \tag{2.6}$$

If we couple the fluid displacement and the solid displacement at the boundary, we can set two boundary conditions. First one, is the no void is created between the solid and fluid, so that, the transmission conditions is:

$$\mathbf{v}_{fluid} \cdot \hat{n}_{fluid} = \mathbf{v}_{solid} \cdot \hat{n}_{solid} \tag{2.7}$$

We know that the the incident a the difracted waves, create no normal velocity on the solid boundary, so that.

$$\frac{\partial\hat{\phi}_0}{\partial r} = -\frac{\partial\hat{\phi}_d}{\partial r} \quad \text{on} \quad \hat{r} = 1 \tag{2.8}$$

As the outer surface is a circle, using the previous equation 2.8, the velocity potential definition and the radial displacement of the solid, working in polar coordinates, we can write it as:

$$\frac{\partial\hat{\phi}_r}{\partial r} = \frac{\partial\hat{w}}{\partial t} \quad \text{on} \quad \hat{r} = 1 \tag{2.9}$$

2.3 Shockwave

In this work we have supposed the shockwave to be cylindrical. In fact this is a simplification for the study in two dimension from the general case of a spherical shockwave in 3D. In (Iakovlev, 2006, Appendix B,) the author obtains the 2D expression for the shockwave, that is expressed as:

$$\phi_0 = -\frac{\lambda p_\alpha (R_0 - r_0)}{\rho_f R} e^{-\frac{(t - c_f^{-1}(R-(R_0-r_0)))}{\lambda}} H(t - c_f^{-1}(R - (R_0 - r_0))) \tag{2.10}$$

and,

$$p_0 = -\frac{p_\alpha (R_0 - r_0)}{R} e^{-\frac{(t - c_f^{-1}(R-(R_0-r_0)))}{\lambda}} H(t - c_f^{-1}(R - (R_0 - r_0))) \tag{2.11}$$

where

$$R = \sqrt{R_0^2 + r^2 - 2R_0 r \cos\theta} \tag{2.12}$$

2.4 Diffracted and Radiated wave

As we can see in Iakovlev (2008a) in order to obtain the diffraction and radiation pressure, we can apply the Laplace transform time-wise to the equation 2.2 in radial coordinates, and we obtain:

$$\frac{\partial^2 \hat{\Phi}}{\partial r^2} + \frac{1}{r}\frac{\partial \hat{\Phi}}{\partial r} + \frac{1}{r^2}\frac{\partial^2 \hat{\Phi}}{\partial \theta^2} - s^2 \hat{\Phi} = 0 \tag{2.13}$$

Where $\hat{\Phi}$ is the Laplace transform of $\hat{\phi}$, and s is the transform variable. Then we use separation on the spatial variables to obtain the general solution of 2.13 imposing the zero condition on $r \to \infty$. This general solution can be written as.

$$\hat{\Phi} = A_n K_n(rs) \cos n\theta \tag{2.14}$$

Where K_n is the modified Bessel function of the second kind of order n and A_n is an arbitrary function of s. If we expand the normal velocity and the normal displacement in series, we can write them as:

$$\left.\frac{\partial \hat{\phi}_0}{\partial r}\right|_{r=1} = \sum_{n=0}^{\infty} b_n(t) \cos n\theta \tag{2.15}$$

and

$$w = \sum_{n=0}^{\infty} w_n(t) \cos n\theta \tag{2.16}$$

Now imposing the boundary conditions we can write the Laplace transform of the harmonics of the unknown potentials as:

$$\hat{\Phi}_{d_n} = B_n \Xi_n \cos n\theta \tag{2.17}$$

$$\hat{\Phi}_{r_n} = sW_n \Xi_n \cos n\theta \tag{2.18}$$

Where B_n and W_N are the Laplace transform of the b_n and w_n coefficients respectively, and Ξ_n is the Laplace transform of what we will call the response function of the problem, ξ_n, and is defined as:

$$\Xi_n(\hat{r}, s) = -\frac{K_n(\hat{r}s)}{sK_n'(s)} \tag{2.19}$$

If we evaluate the response function at the boundary ($\hat{r} = 1$), we can write it as:

$$\Psi_n(s) = -\frac{K_n(s)}{sK_n'(s)} \tag{2.20}$$

The response functions represents the response of the external fluid to the motion of the solid. As we can see, they are independent of the solid properties, and do only depend on the problem geometry. This will be the key of our analytical approach. Once we obtain the response functions for any given geometry, we can use them to solve any material configuration at any time step. This makes this approach very interesting in terms of computational efficiency. The response functions ξ_n represents the volume response functions, where we relate the displacement in the solid with the effect anywhere in the fluid. Meanwhile the ψ_n response function is the restriction over the boundary and is the one to be used when coupling the solid deformation and the effect on the fluid.

We must remember that pressure p and potential ϕ are related, and we can write this relation as

$$p = -\rho_f \frac{\partial \phi}{\partial t} \Rightarrow \hat{p} = -\frac{\partial \hat{\phi}}{\partial t} \tag{2.21}$$

Using Fourier decomposition on the pressure we can write the whole formulation for the pressure as:

$$\hat{p}_d = \sum_{n=0}^{\infty} \hat{p}_{d_n} \cos n\theta \tag{2.22}$$

$$\hat{p}_r = \sum_{n=0}^{\infty} \hat{p}_{r_n} \cos n\theta \tag{2.23}$$

$$\hat{p}_0 = \sum_{n=0}^{\infty} \hat{p}_{0_n} \cos n\theta \tag{2.24}$$

$$\hat{p} = \sum_{n=0}^{\infty} \hat{p}_n \cos n\theta \tag{2.25}$$

And total pressure harmonics $\hat{p}_n$ can be written as:

$$\hat{p}_n = \hat{p}_{0_n} + \hat{p}_{d_n} + \hat{p}_{r_n} \tag{2.26}$$

Using some Laplace transform related theorems, the diffraction and radiation terms can be written as

$$\hat{p}_{d_n} = -\frac{1}{\sqrt{r}} b_n(\hat{t}) - \int_0^{\hat{t}} b_n(\eta) \frac{d\xi_n}{d\eta}(\hat{r}, \hat{t} - \eta) d\eta \tag{2.27}$$

and

$$\hat{p}_{r_n} = \int_0^{\hat{t}} \frac{d^2 w_n(\eta)}{d\eta^2} \xi_n(\hat{r}, \hat{t} - \eta) d\eta \tag{2.28}$$

As we are interested in the interaction with the solid, we can bound the computations on the outer edge of the solid ($\hat{r} = 1$) so that, as we have defined $\psi(\hat{t}) = \xi_n(1, \hat{t})$

$$\hat{p}_{r_n} = \int_0^{\hat{t}} \frac{d^2 w_n(\eta)}{d\eta^2} \psi_n(\hat{t} - \eta) d\eta \tag{2.29}$$

Using integration by parts we can write equation 2.29 in a different form, using velocities instead of accelerations, and the response function first time derivative.

$$\hat{p}_{r_n} = \left[\frac{dw_n(\eta)}{d\eta} \psi_n(\hat{t} - \eta) \right]_0^{\hat{t}} + \int_0^{\hat{t}} \frac{dw_n(\eta)}{d\eta} \frac{\psi_n(\hat{t} - \eta)}{d\eta} d\eta \tag{2.30}$$

Changing notation as $\frac{df}{dt} = \dot{f}$, and using $\psi(0) = 1$ we can write it as:

$$p_{r_n} = \dot{w}_n(\hat{t}) + \int_0^{\hat{t}} \dot{w}_n(\eta) \dot{\psi}_n(\hat{t} - \eta) d\eta \tag{2.31}$$

And as p_0 is known from our shockwave then we can relate the global pressure harmonics and the harmonics of the displacement of the outer boundary of our solid.

We must point out that not only p_0 is known, p_d does only depend on the response functions and the incident shockwave, so that they are independent on the solid displacements and are fixed for a given geometry.

We can use this fact to compute the shockwave for any given geometry (incident and diffracted values) and the only term that will change depending on our solid properties and behavior is $\hat{p}_{r_n}$.

Chapter 3

Modelling the Solid

3.1 Hypothesis

In the present work some simplifications about the solid behavior have been made also. They are common simplifications in structural dynamics and perform very well inside their field of application, enabling a much lower computational cost. It is left for further work to deal with more general assumptions.

The first assumption is that we can reduce our study to a 2D study omitting the third dimension. This is due either because the solid is very thin and has no actions outside its middle plane (plane stress) or either the solid is extremely long and deformations in the third directions are 0 due to the symmetry (plane strain).

The second assumption that has been made is that the deformed and the original geometry are almost the same, so the deformations are small.

The third assumption that has been made is that each material that constitute the solid is homogenous and isotropic. Its properties are exactly the same all over the material and in any direction.

The fourth assumption that has been made is that the material behaves as a perfectly elastic material where the stresses are proportional to the strains.

And at last, it has also been assumed Rayleigh type dumping.

3.2 Governing equations

Starting from the continuum mechanics equations, the first equation that will describe the solid behavior is the momentum conservation.

$$\nabla \cdot \sigma + b = \rho \frac{d^2 u}{dt^2} \tag{3.1}$$

from the small deformations assumption we define the strain tensor as:

$$\epsilon = \nabla^s u \tag{3.2}$$

The material is also assumed to be linearly elastic so for a given elastic fourth order tensor $\mathbb{C}$ we can write the stress tensor as function of the strain tensor.

$$\sigma = \mathbb{C} : \epsilon \tag{3.3}$$

As the material is isotropic, we can write the $\mathbb{C}$ constitutive tensor as:

$$\mathbb{C} = \lambda \mathbb{1} \otimes \mathbb{1} + 2\mu \mathbb{I} \tag{3.4}$$

where $\mathbb{1}$ is the identity matrix and:

$$\mathbb{I}_{ijkl} = \frac{1}{2}(\delta_{ik}\delta_{jl} + \delta_{il}\delta_{jk})$$

And we can relate the λ and μ coefficients with the more common in engineering Young Modulus (E) and Poisson coefficient (ν).

$$\lambda = \frac{\nu E}{(1+\nu)(1-2\nu)} \tag{3.5}$$

$$\mu = \frac{E}{2(1+\nu)} \tag{3.6}$$

We must stress out also that the sound propagation speed in the solid (c_s)can be related to the Young Modulus (E), density (ρ_s) and the Poisson coefficient (ν) by:

$$c_s = \sqrt{\frac{E}{\rho_s(1-\nu^2)}} \tag{3.7}$$

As we are under plane stress/plane strain simplifications, we can simplify the both the strain and stress tensors to three component vectors:

$$\epsilon = \begin{pmatrix} \epsilon_{xx} \\ \epsilon_{yy} \\ \gamma_{xy} \end{pmatrix}$$

$$\sigma = \begin{pmatrix} \sigma_{xx} \\ \sigma_{yy} \\ \sigma_{xy} \end{pmatrix}$$

And we can relate them using a constitutive matrix D that depends on if we are under Plane Stress / Plane Strain assumptions.

Plane Stress:

$$D = \begin{pmatrix} \frac{E}{1-\nu^2} & \frac{\nu E}{1-\nu^2} & 0 \\ \frac{\nu E}{1-\nu^2} & \frac{E}{1-\nu^2} & 0 \\ 0 & 0 & \frac{E}{2(1+\nu)} \end{pmatrix} \tag{3.8}$$

Plane Strain:

$$D = \begin{pmatrix} \frac{E(1-\nu)}{(1-2\nu)(1+\nu)} & \frac{\nu E}{(1-2\nu)(1+\nu)} & 0 \\ \frac{\nu E}{(1-2\nu)(1+\nu)} & \frac{E(1-\nu)}{(1-2\nu)(1+\nu)} & 0 \\ 0 & 0 & \frac{E}{2(1+\nu)} \end{pmatrix} \tag{3.9}$$

And we can write the stress-strain relation as:

$$\sigma = D\epsilon \tag{3.10}$$

3.3 Finite Element Method Scheme

For modeling the solid, we have used the Finite Element Method. It is not the intention of the present work to dive inside a so well known method with such an extense bibliography available. We will focus on the very basics and the main ideas. Further information can be found in Oñate (2004).

The key of this method is to discretize our domain into small portions, that will be called elements. so that inside each element the value of our displacement will be given by interpolation of the value on the nodes.

We call nodes to the base points of our discretization that are going to define our approximation. We are going to choose shape functions so that the shape function N_i has value 1 on node i, and 0 on the other nodes. We can write it as:

$$N_i(x_j) = \begin{cases} 1 & i = j \\ 0 & i \neq j \end{cases} \tag{3.11}$$

We can approximate our displacement field as :

$$u \approx \sum_{i=1}^{n} N_i(x) u_i \tag{3.12}$$

When computing, our starting point is the weak form of the equilibrium equation, also known as Virtual Work Principle.

$$\int_\Omega \delta\epsilon^T \sigma d\Omega + \int_\Omega \delta u^T \rho \frac{d^2u}{dt^2} d\Omega = \int_\Omega \delta u^T b d\Omega + \int_{\partial\Omega} \delta u^T p d\Gamma \tag{3.13}$$

Where δu is the virtual displacement field imposed to body, and $\delta\epsilon$ is the strain field generated by it.

We define the components of the strain vector as:

$$\epsilon_{xx} = \frac{\partial u^x}{\partial x} \tag{3.14}$$

$$\epsilon_{yy} = \frac{\partial u^y}{\partial y} \tag{3.15}$$

$$\gamma_{xy} = \frac{\partial u^x}{\partial y} + \frac{\partial u^y}{\partial x} \tag{3.16}$$

As we are approximating the displacement field with the shape functions, we can rewrite the strain field as a function of them.

$$\epsilon_{xx} = \sum_{i=1}^{n} \frac{\partial N_i}{\partial x} u_i^x \tag{3.17}$$

$$\epsilon_{yy} = \sum_{i=1}^{n} \frac{\partial N_i}{\partial y} u_i^y \tag{3.18}$$

$$\gamma_{xy} = \sum_{i=1}^{n} \frac{\partial N_i}{\partial y} u_i^x + \sum_{i=1}^{n} \frac{\partial N_i}{\partial x} u_i^y \tag{3.19}$$

$$\tag{3.20}$$

So we can write both fields in a matricial way:

$$u = \begin{pmatrix} u^x \\ u^y \end{pmatrix} = \sum_{i=1}^{n} \begin{pmatrix} N_i & 0 \\ 0 & N_i \end{pmatrix} \begin{pmatrix} u_i^x \\ u_i^y \end{pmatrix} \tag{3.21}$$

and

$$\epsilon = \begin{pmatrix} \epsilon_{xx} \\ \epsilon_{yy} \\ \gamma_{xy} \end{pmatrix} = \sum_{i=1}^{n} \begin{pmatrix} \frac{\partial N_i}{\partial x} & 0 \\ 0 & \frac{\partial N_i}{\partial y} \\ \frac{\partial N_i}{\partial y} & \frac{\partial N_i}{\partial x} \end{pmatrix} \begin{pmatrix} u_i^x \\ u_i^y \end{pmatrix} \tag{3.22}$$

We can rearrange the terms of the sum in a single matrix product

$$u = \left(\begin{array}{cc|cc|c|cc} N_1 & 0 & N_2 & 0 & \cdots & N_n & 0 \\ 0 & N_1 & 0 & N_2 & \cdots & 0 & N_n \end{array}\right) \begin{pmatrix} u_1^x \\ u_1^y \\ u_2^x \\ \vdots \\ u_n^x \\ u_n^y \end{pmatrix} \tag{3.23}$$

So that,

$$u = NU \tag{3.24}$$

and

$$\epsilon = \left(\begin{array}{cc|cc|c|cc} \frac{\partial N_1}{\partial x} & 0 & \frac{\partial N_2}{\partial x} & 0 & \cdots & \frac{\partial N_n}{\partial x} & 0 \\ 0 & \frac{\partial N_1}{\partial y} & 0 & \frac{\partial N_2}{\partial y} & \cdots & 0 & \frac{\partial N_n}{\partial y} \\ \frac{\partial N_1}{\partial y} & \frac{\partial N_1}{\partial x} & \frac{\partial N_2}{\partial y} & \frac{\partial N_2}{\partial x} & \cdots & \frac{\partial N_n}{\partial y} & \frac{\partial N_n}{\partial x} \end{array}\right) \begin{pmatrix} u_1^x \\ u_1^y \\ u_2^x \\ \vdots \\ u_n^x \\ u_n^y \end{pmatrix} \tag{3.25}$$

Therefore,

$$\epsilon = BU \tag{3.26}$$

So we can write the weak form as:

$$\int_\Omega \delta U^T B^T D B U d\Omega + \int_\Omega \delta U^T \rho N^T N \frac{d^2U}{dt^2} d\Omega = \int_\Omega \delta U^T N^T b d\Omega + \int_{\partial\Omega} \delta U^T N^T p d\Gamma \tag{3.27}$$

as we suppose there are no other forces than the impact of the shockwave, we can rewrite the whole equation as:

$$\delta U^T \left(\underbrace{\int_\Omega B^T D B d\Omega}_{K} U + \underbrace{\int_\Omega \rho N^T N d\Omega}_{M} \ddot{U} \right) = \delta U^T \left(\underbrace{\int_\Omega N^T b d\Omega}_{0} + \underbrace{\int_{\partial\Omega} N^T p d\Gamma}_{F} \right) \tag{3.28}$$

So that we can write the discrete version of the momentum conservation equation as:

$$M\ddot{U} + KU = F \tag{3.29}$$

We add a dissipation term,

$$M\ddot{U} + C\dot{U} + KU = F \tag{3.30}$$

As we have pointed out, this new added dumping term is supposed to be follow a Rayleigh decomposition, so that:

$$C = c_1 M + c_2 K \tag{3.31}$$

We have to stress out that we are not going to build the whole matrix N or B, nor we are going to compute the integrals analytically. We are going to use numerical integration and ensamble K and M matrices directly using the contribution of each element, knowing that on each element only the nodes included in it have a contribution on K or M.

3.4 Actions over the solid

Due to the nature of our actions, we are going to neglect the body forces distributed all over the solid, and also the hydrostatic pressure of the fluid surrounding the body. As we are in small deformations and linear elasticity theory, we can focus only on the variations with respect to the steady state. So that, for instance, the flotation of the solid is not checked, and is assumed.

In our work we have supposed the solid to be evacuated, so there is no inner fluid and therefore no inner pressure. Then, the effect of the shockwave over the solid can be reduced to a total pressure distribution all over the outer boundary.

As we will see later on, the total pressure will be defined in the outer nodes of our solid, so we must interpolate the pressure over the boundary to obtain an approximated pressure distribution. Then ir order to reduce it to the effect over the outer nodes, we must integrate it over the element outer boundary.

This is achieved supposing linear interpolation. For a given element face that connects nodes a and b, we have its length l_{ab} and its outward unitary normal n_{ab}, we can write the contribution over these nodes as:

$$F_a^{ab} = n_{ab} l_{ab} \left(\frac{p_a}{3} + \frac{p_b}{6} \right) \tag{3.32}$$

$$F_b^{ab} = n_{ab} l_{ab} \left(\frac{p_b}{3} + \frac{p_a}{6} \right) \tag{3.33}$$

So in order to compute the independent term, we just have to sum the contribution of all the faces to the nodes that are forming them.

3.5 Time integration

From now on we are going to denote U_n as the displacements on the nodes on instant n, and we are supposing a constant time step discretization Δt.

For the time integration we are going to use the Newmark method. This method is based in approximating both first and second derivatives in time as a function of the value and previos time steps values.

Starting from:

$$U_{n+1} = U_n + \Delta t \dot{U}_n + \frac{\Delta t^2}{2}\left(\left(1-2\beta\right)\ddot{U}_n + 2\beta\ddot{U}_{n+1}\right) \tag{3.34}$$

$$\dot{U}_{n+1} = \dot{U}_n + \Delta t\left(\left(1-\gamma\right)\ddot{U}_n + \gamma\ddot{U}_{n+1}\right) \tag{3.35}$$

We get the expression of $\ddot{U}_{n+1}$ and $\dot{U}_{n+1}$

$$\ddot{U}_{n+1} = \frac{1}{\beta\Delta t^2}\left(U_{n+1} - U_n - \Delta t\dot{U}_n\right) - \left(\frac{1}{2\beta} - 1\right)\ddot{U}_n \tag{3.36}$$

$$\dot{U}_n + 1 = \frac{\gamma}{\beta\Delta t}\left(U_{n+1} - U_n\right) - \left(\frac{\gamma}{\beta} - 1\right)\dot{U}_n - \Delta t\left(\frac{\gamma}{2\beta} - 1\right)\ddot{U}_n \tag{3.37}$$

If we substitute it in equation 3.30 we obtain:

$$\begin{aligned} KU_{n+1} + \frac{\gamma}{\beta\Delta t}CU_{n+1} + \frac{1}{\beta\Delta t^2}MU_{n+1} = F_{n+1} + \\ +C\left(\frac{1}{2\beta\Delta t}U_n + \left(\frac{\gamma}{2\beta} - 1\right)\dot{U}_n + \frac{\Delta t}{2}\left(\frac{\gamma}{2\beta} - 2\right)\ddot{U}_n\right) \\ +M\left(\frac{1}{2\beta\Delta t^2}U_n + \frac{1}{2\beta\Delta t}\dot{U}_n + \left(\frac{1}{4\beta} - 1\right)\ddot{U}_n\right) \end{aligned} \tag{3.38}$$

Defining:

$$K^* = K + \frac{\gamma}{\beta\Delta t}C + \frac{1}{\beta\Delta t^2}M \tag{3.39}$$

$$\begin{aligned} F^*_{n+1} = F_{n+1} + C\left(\frac{1}{2\beta\Delta t}U_n + \left(\frac{\gamma}{2\beta} - 1\right)\dot{U}_n + \frac{\Delta t}{2}\left(\frac{\gamma}{2\beta} - 2\right)\ddot{U}_n\right) + \\ +M\left(\frac{1}{2\beta\Delta t^2}U_n + \frac{1}{2\beta\Delta t}\dot{U}_n + \left(\frac{1}{4\beta} - 1\right)\right) \end{aligned} \tag{3.40}$$

So we can write the equation 3.38 just as:

$$K^*U_{n+1} = F^*_{n+1} \tag{3.41}$$

And from $U_{n+1}, U_n, \dot{U}_n, \ddot{U}_n$ we can reconstruct and obtain $\dot{U}_{n+1}$ and $\ddot{U}_{n+1}$.

Chapter 4

Coupling the Fluid and the Solid models

In the present chapter we are going to introduce how the coupling between the fluid model and the solid model is done. For the coupling we are using a staggered approach that has been tested to be robust and to provide accurate enough results.

The weak coupling or staggered approach consists on computing explicitly the pressure on the fluid using as a starting point the velocity field in the solid the previous step.

Then we use the computed Pressure field over the solid boundary in order to obtain the forces and computing the solid displacements and velocities.

Then we start the procedure again for the next time step. We can see the representation of the scheme in figure 4.1.

Coupling has been the main issue in the present work, because the solid and the fluid model work in complete different ways.

The first drawback is that points where the fluid properties and the solid properties are defined (mesh) do not necessarily match. That means in order to transfer information from one model to another we have to interpolate information in an efficient way.

The second one is that while the solid model works in cartesian coordinates, the fluid model works in polar coordinates. So that we must implement an efficient way to translate from cartesian to polar coordinates.

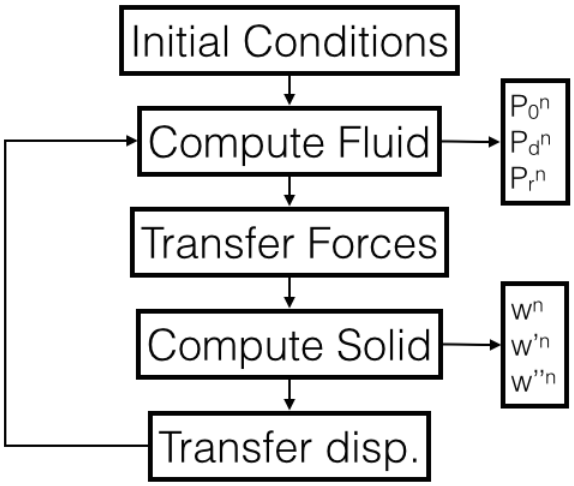

Figure 4.1: Time Iteration Scheme

The last one, but also the most complex one is that solid model works in a spatial distribution of values, while fluid model works with the Fourier decomposition of the values over the boundary. So that we need to perform Fourier integration and decomposition at each time step.

In figure 4.2 we can see a complete scheme of the procedure, including the need transformations in data.

4.1 Input and Output parameters on the Fluid

The fluid is characterized by its density ρ_f and its fluid sound velocity c_f, and the shockwave is characterized by the initial position the decay and the peak pressure R_0, λ, p_α. With these data we can compute at each time both incident pressure (p_0) and diffracted pressure (p_d), that do only depend on the outer shape of solid (and is always the same), so we can compute them once and use them for all the simulations that match the shockwave.

From them, we have to compute at each time step the radiated pressure (p_r). For computing so, we need the response function ψ and the fluid interface radial velocity ($\dot{w}$). In fact we work in Fourier decompositions so we need their Fourier coefficients.

- INPUT: $\dot{w}_n|_{FLUID}$ Fourier terms of the radial velocity on the fluid mesh.

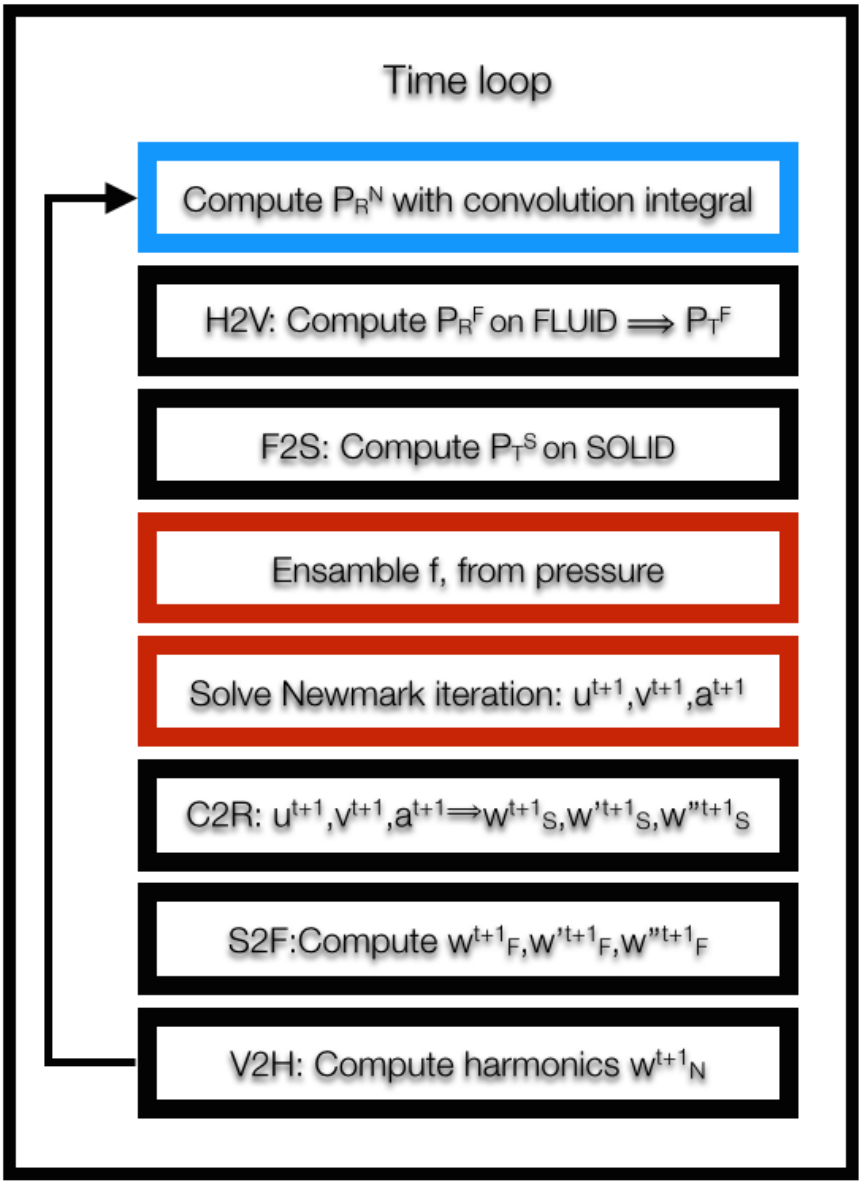

Figure 4.2: Complete Algorithm

- OUPUT: $p_{rn}|_{FLUID}$ Fourier terms of the radiated pressure on the fluid mesh.

4.2 Input and Output parameters on the Solid

The solid is characterized by its elastic parameters E, ν and its density ρ_s. With these parameters we can obtain the sound velocity in the solid c_s. For the given geometry

(and its partition or mesh) we can ensamble the stiffness matrix K, the mass matrix M the dumping matrix C and using Newmark's method combine them for obtaining K^*. But at each time step we need to compute the acting forces over the solid and they depend on the total pressure, so it is our input parameter for the coupling. As a result from solving the motion, we obtain $u, v, \dot{u}, \dot{v}, \ddot{u}, \ddot{v}$.

- INPUT: $p|_{SOLID}$ Total pressure on the solid mesh.
- OUPUT: $u, v, \dot{u}, \dot{v}, \ddot{u}, \ddot{v}|_{SOLID}$ Displacements, velocities and acceleration in cartesian coordinates.

4.3 From fluid to solid mesh (and viceversa). Interpolating membrane

As we have seen in previous sections fluid and solid meshes do not necessarily match. And coupling parameters on both solid and fluid model are defined in them, we have to develop an efficient way to transfer values between meshes.

Our inspiration has been to create a mathematical interface containing the position of the nodes of both meshes. So that we can fix the values on one mesh and then interpolate the values on the other mesh, so we when we transfer from solid to fluid, we fix the values on the solid and then interpolate the values on the fluid.

As we have to perform this operation at each time step, we developed an efficient way to deal with this interpolation.

We used shape functions, so that any shape on any mesh could be written as combination of these shape functions, so we can write the values of the shape functions on the other mesh. Thus for any set of values on one mesh, we can compute the values on the other mesh as the sum of the contribution of the shape functions times the value at the initial point.

$$u_{M1} = \sum_{i=1}^{n_1} U^i_{M1} N^i_{M1} \tag{4.1}$$

$$\hat{u}^{i,j}_{M2} = N^j_{M1}(\theta_i) \quad i = 1, \ldots, n_2 \tag{4.2}$$

Using this decomposition we can write it in a matrix way.

$$U_{M2} = \begin{pmatrix} \hat{u}_{M2}^{1,1} & \hat{u}_{M2}^{1,2} & \cdots & \hat{u}_{M2}^{1,n_1} \\ \vdots & & & \vdots \\ \hat{u}_{M2}^{n_2,1} & \hat{u}_{M2}^{n_2,2} & \cdots & \hat{u}_{M2}^{n_2,n_1} \end{pmatrix} \begin{pmatrix} U_{M1}^1 \\ U_{M1}^2 \\ \cdots \\ U_{M1}^{n_1} \end{pmatrix} \tag{4.3}$$

So once we obtain both matrices we can transfer fields from one mesh to the other just by multiplying them by a matrix. So at the very beginning we compute both matrices.

- I_{FS}: Matrix that transforms values from fluid mesh to solid mesh
- I_{SF}: Matrix that transforms values from solid mesh to fluid mesh

So that,

$$V_{fluid} = I_{SF} V_{solid} \tag{4.4}$$

$$V_{solid} = I_{FS} V_{fluid} \tag{4.5}$$

4.4 From cartesian to polar coordinates

As we have seen previously, we obtain the displacements and velocities in the solid in cartesian coordinates, but then we need the radial displacement and velocities to compute the radiated pressure.

For doing so, we have computed at first step our outer circle center. It is used also as a verification, so that the outer shape is circular and no other outer shapes are used. From the computed center, we compute the outward unitary radial vectors. From then we compute the projection of unitary vectors in both x and y over those directions (keeping track of the point they belong to).

So for any point if we denote the unitary vector in the radial direction as $v_j = (v_j^x, v_j^y)$ and if we denote any value in cartesian coordinates $c_j = (c_j^x, c_j^y)$. We can compute the radial projection of c_j as.

$$c_j|_{radial} = c_j^x v_j^x + c_j^y v_j^y \tag{4.6}$$

So that we can compute it in a matricial way as:

$$c|_{radial} = \begin{pmatrix} v_1^x, & \cdots & , v_n^x \end{pmatrix} \begin{pmatrix} c_1^x \\ \vdots \\ c_n^x \end{pmatrix} + \begin{pmatrix} v_1^y, & \cdots & , v_n^y \end{pmatrix} \begin{pmatrix} c_1^y \\ \vdots \\ c_n^y \end{pmatrix} \tag{4.7}$$

So we can achieve that conversion multiplying x and y values by matrices I^x_{CP} and I^y_{CP} and adding the results. Those matrices are the cartesian to radial conversion matrices.

$$c|_{radial} = I^x_{CP} \begin{pmatrix} c^x_1 \\ \vdots \\ c^x_n \end{pmatrix} + I^y_{CP} \begin{pmatrix} c^y_1 \\ \vdots \\ c^y_n \end{pmatrix} \tag{4.8}$$

where,

$$I^x_{CP} = diag \begin{pmatrix} v^x_1, & \cdots & , v^x_n \end{pmatrix} \tag{4.9}$$

$$I^y_{CP} = diag \begin{pmatrix} v^y_1, & \cdots & , v^y_n \end{pmatrix} \tag{4.10}$$

4.5 Harmonic decomposition and reconstruction

The last thing we have to solve for effectively coupling the fluid and solid model is being able to effectively switch between nodal values and harmonics and viceversa. If we recall the expression in harmonics.

$$f(\theta) = \frac{f_0}{2} + \sum_{n=1}^{\infty} f^c_n \cos n\theta + \sum_{n=1}^{\infty} f^s_n \sin n\theta \tag{4.11}$$

We can approximate any function by a finite number of harmonics, the more harmonics we use, the more accurate it is. So for a given number of harmonics n_h.

$$f(\theta) \approx \frac{f_0}{2} + \sum_{n=1}^{n_h} f^c_n \cos n\theta + \sum_{n=1}^{n_h} f^s_n \sin n\theta \tag{4.12}$$

4.5.1 Harmonic reconstruction. From harmonics to values over the mesh

If we define a vector where we store all the harmonic values

$$f_{harmonic} = \begin{pmatrix} f_0 \\ f^c_1 \\ \vdots \\ f^c_{n_h} \\ f^s_1 \\ \vdots \\ f^s_{n_h} \end{pmatrix} \tag{4.13}$$

By construction, we can check that we can obtain the values over the mesh (defined by angles $\theta_1, \ldots, \theta_n$) as:

$$\begin{pmatrix} f(\theta_1) \\ \vdots \\ f(\theta_n) \end{pmatrix} = \begin{pmatrix} 1/2 & \cos\theta_1 & \ldots & \cos n_h\theta_1 & \sin\theta_1 & \ldots & \sin n_h\theta_1 \\ \vdots & & & & & & \vdots \\ 1/2 & \cos\theta_n & \ldots & \cos n_h\theta_n & \sin\theta_n & \ldots & \sin n_h\theta_n \end{pmatrix} \begin{pmatrix} f_0 \\ f_1^c \\ \vdots \\ f_{n_h}^c \\ f_1^s \\ \vdots \\ f_{n_h}^s \end{pmatrix} \tag{4.14}$$

So that we can rename them as

$$f_{mesh} = I_{HV} f_{harmonics} \tag{4.15}$$

4.5.2 Harmonic decomposition. From values over the mesh to harmonics

From Fourier series theory we know that we can compute the terms in equation 4.11 as

$$f_0 = \frac{1}{\pi}\int_{-\pi}^{\pi} f(\theta)d\theta \tag{4.16}$$

$$f_n^c = \frac{1}{\pi}\int_{-\pi}^{\pi} f(\theta)\cos n\theta d\theta \tag{4.17}$$

$$f_n^s = \frac{1}{\pi}\int_{-\pi}^{\pi} f(\theta)\sin n\theta d\theta \tag{4.18}$$

As we are using linear interpolation over the outer circle, we can write $f(\theta)$ as an approximation with interpolation functions. With $N_i(\theta)$ is the shape function for θ_i

$$f(\theta) \approx \sum_{i=1}^{n_p} f_i N_i(\theta) \tag{4.19}$$

Then we can rewrite the previos equations as:

$$f_0 = \frac{1}{\pi}\int_{-\pi}^{\pi}\left(\sum_{i=1}^{n_p} f_i N_i(\theta)\right) d\theta \tag{4.20}$$

$$f_n^c = \frac{1}{\pi}\int_{-\pi}^{\pi}\left(\sum_{i=1}^{n_p} f_i N_i(\theta)\right) \cos n\theta d\theta \tag{4.21}$$

$$f_n^s = \frac{1}{\pi}\int_{-\pi}^{\pi}\left(\sum_{i=1}^{n_p} f_i N_i(\theta)\right) \sin n\theta d\theta \tag{4.22}$$

Re-arranging terms:

$$f_0 = \sum_{i=1}^{n_p} f_i \left(\frac{1}{\pi}\int_{-\pi}^{\pi} N_i(\theta) d\theta\right) \tag{4.23}$$

$$f_n^c = \sum_{i=1}^{n_p} f_i \left(\frac{1}{\pi}\int_{-\pi}^{\pi} N_i(\theta)\cos n\theta d\theta\right) \tag{4.24}$$

$$f_n^s = \sum_{i=1}^{n_p} f_i \left(\frac{1}{\pi}\int_{-\pi}^{\pi} N_i(\theta)\sin n\theta d\theta\right) \tag{4.25}$$

As we are using linear interpolation, If we define $\Delta_{i,j} = \theta_j - \theta_i$, and we suppose $\theta_1 < \theta_2 < \ldots < \theta_{n_p}$ we can write $N_i(\theta)$ as:

$$N_i(\theta) = \begin{cases} \dfrac{(\theta - \theta_{i-1})}{\Delta_{i-1,i}} \text{ if } \theta_{i-1} < \theta \leq \theta_i \\ \dfrac{(\theta_{i+1} - \theta)}{\Delta_{i,i+1}} \text{ if } \theta_{i-1} < \theta < \theta_i \\ \qquad 0\text{Otherwise} \end{cases} \tag{4.26}$$

Then we can compute the integrals analytically:

$$\int_{-\pi}^{\pi} N_i(\theta)\cos n\theta d\theta = \int_{\theta_{i-1}}^{\theta_i} \frac{(\theta - \theta_{i-1})}{\Delta_{i-1,i}}\cos n\theta d\theta + \int_{\theta_i}^{\theta_{i+1}} \frac{(\theta_{i+1} - \theta)}{\Delta_{i,i+1}}\cos n\theta d\theta \tag{4.27}$$

$$N_c^{i,n} = \int_{-\pi}^{\pi} N_i(\theta)\cos n\theta d\theta = \frac{[n\theta\sin n\theta + \cos n\theta - \theta_{i-1} n\sin n\theta]_{\theta_{i-1}}^{\theta^i}}{n^2\Delta_{i-1,i}} - \frac{[n\theta\sin n\theta + \cos n\theta - \theta_{i+1} n\sin n\theta]_{\theta_i}^{\theta^{i+1}}}{n^2\Delta_{i,i+1}} \tag{4.28}$$

In the same way:

$$N_s^{i,n} = \int_{-\pi}^{\pi} N_i(\theta) \sin n\theta d\theta = \frac{[\sin n\theta - n\theta \cos n\theta + \theta_{i-1} n \cos n\theta]_{\theta_{i-1}}^{\theta^i}}{n^2 \Delta_{i-1,i}} - \frac{[\sin n\theta - n\theta \cos n\theta + \theta_{i+1} n \cos n\theta]_{\theta_i}^{\theta^{i+1}}}{n^2 \Delta_{i,i+1}} \tag{4.29}$$

$$N_0^{i,n} = \int_{-\pi}^{\pi} N_i(\theta) d\theta = \left[\frac{\theta^2/2 - \theta_{i-1}\theta}{\Delta_{i-1,i}}\right]_{\theta_{i-1}}^{\theta_i} - \left[\frac{\theta^2/2 - \theta_{i+1}\theta}{\Delta_{i,i+1}}\right]_{\theta_i}^{\theta_{i+1}} \tag{4.30}$$

So we can write it in a matrix form as:

$$\begin{pmatrix} f_0 \\ f_1^c \\ \vdots \\ f_{n_h}^c \\ f_1^s \\ \vdots \\ f_{n_h}^s \end{pmatrix} = \begin{pmatrix} N_0^1 & N_0^2 & \cdots & N_0^{n_p} \\ N_c^{1,1} & N_c^{2,1} & \cdots & N_c^{n_p,1} \\ \vdots & & & \vdots \\ N_c^{1,n_h} & N_c^{2,n_h} & \cdots & N_c^{n_p,n_h} \\ N_s^{1,1} & N_s^{2,1} & \cdots & N_s^{n_p,1} \\ \vdots & & & \vdots \\ N_s^{1,n_h} & N_s^{2,n_h} & \cdots & N_s^{n_p,n_h} \end{pmatrix} \begin{pmatrix} f_1 \\ f_2 \\ \vdots \\ f_n \end{pmatrix} \tag{4.31}$$

Chapter 5

Results and Validation

For all the cases in this chapter we have used the same shockwave and the same fluid properties. As we have pointed out in the previous chapter 2 exactly in sections 2.2 and 2.3, we are using a linearly compressible, inviscid irrotational fluid model, and we are using a exponential peak decay model for the shockwave.

So the fluid and the shockwave are fully determined by:

Fluid		
c_f	$1,470\,m/s$	Sound speed in fluid
Shockwave		
R_0	$4.00\,m$	Position of the shockwave focus
λ	$3.76ms$	Exponential decay
p_α	$25\,kPa$	Peak pressure in the front

We must recall that shockwave comes from the right in our representations so that the the plot point 1 or head is the one in the outer radius when $\theta = 0$ and the plot point 2 or tail is the once in the outer radius when $\theta = \pi$.

5.1 Thin Shell. Validation

As a first example, we have run a simulation using a plain thin shell made of steel. Although previous methods were capable of computing that geometry, we are using this specific geometry as a validation test of our model. We want to reproduce exactly

the same simulation and compare both results in order to ensure the goodness of the results.

The used geometry is a thin steel evacuated pipe with the following characteristics.

Geometry		
r_0	$1.00\,m$	Outer radius
h_0	$0.03\,m$	Thickness
Materials		
E	$4.5895 \cdot 10^{11}\,Pa$	Young Modulus
ν	0.30	Poisson Coefficient
c_s	$7,990\,m/s$	Sound speed in solid
ρ	$7,900\,kg/m^3$	Density

On the next figures we can see first the geometry and the used mesh (figures 5.1 and 5.1). Then we have plotted the displacement in radial direction w both in Head and Tail (figure 5.3) and also its velocities $\dot{w}$ (figure 5.4). In figure 5.7 we can see the total pressure evolution in Head and Tails, while in figures 5.8 and 5.9 we can see the contribution of the incident and the diffracted wave $(p_0 + p_d)$ and the radiated wave (p_r) for both Head and Tail.

In figures 5.5 and 5.6 we can see the plot of our method's result in red compared to the ones using regular Reissner-Meindlin computations. In fact we are comparing radial displacements and radial velocities in the Head point. We can see in figure 5.5 that both results match almost perfectly and in fact both lines are hard to distinguish. In figure 5.6 we have performed the same operation but using the radial velocity $\dot{w}$ instead of w. We can see in this figure that values match very well except for the very late times where we can observe a slight variation in phase (that seems to start much earlier and increase along time) probably due to the change in structure stiffness caused by the FEM discretization.

In figure 5.10 we can see the the reconstruction of the acoustic field for times $\hat{t} = 0.5$, $\hat{t} = 1.2$, $\hat{t} = 1.9$, $\hat{t} = 2.6$, $\hat{t} = 3.3$ and $\hat{t} = 4.0$. We can see how the shockwave arrives from the right and how even when the shockwave has not arrived yet to some parts the fluid are already affected by the radiated pressure.

From then, as the effect of the incident shockwave vanishes in the fluid, we can appreciate the effect of the radiated pressure all over the fluid, for instance in $\hat{t} = 4.0$ he acoustic field is clearly dominated by the vibration of the the solid.

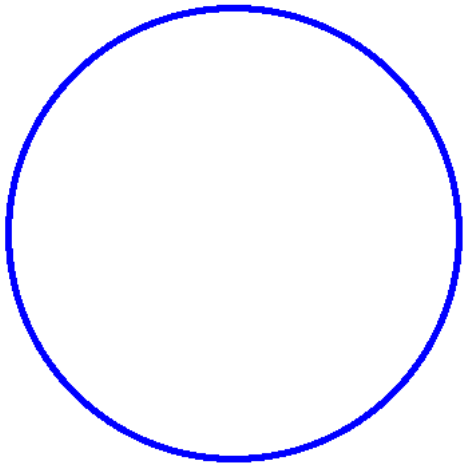

Figure 5.1: Thin Shell. Geometry

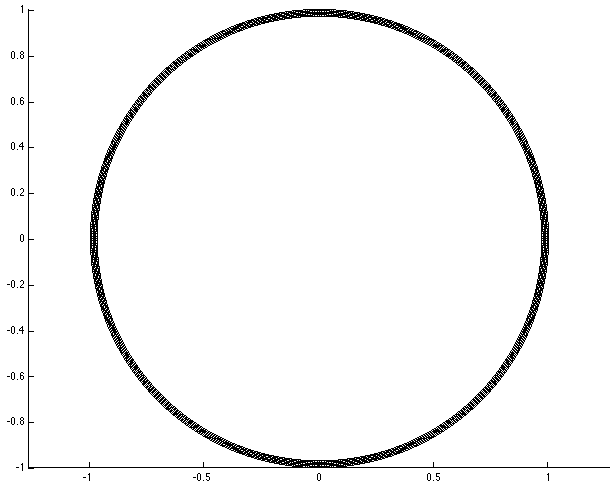

Figure 5.2: Thin Shell. Mesh

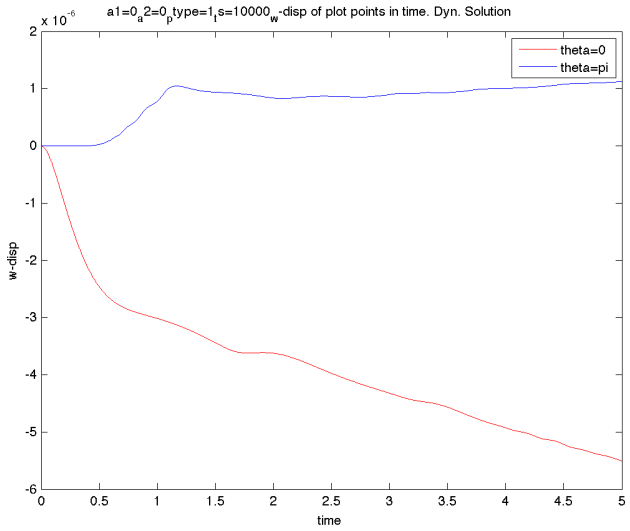

Figure 5.3: Thin Shell. w in Head and Tail

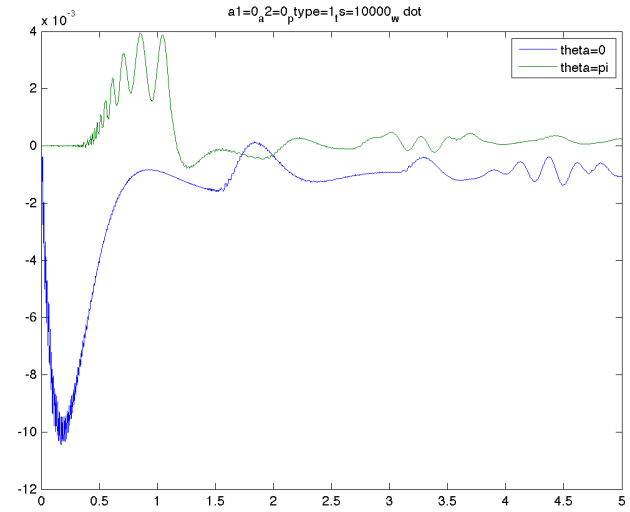

Figure 5.4: Thin Shell. $\dot{w}$ in Head and Tail

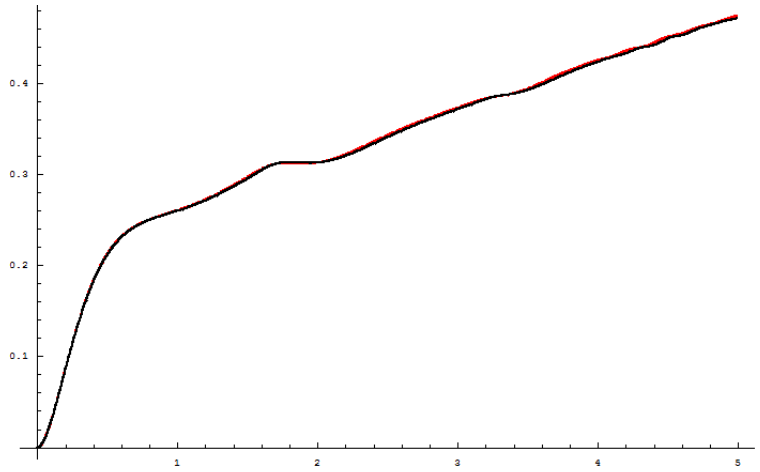

Figure 5.5: Thin Shell. w comparison in Head

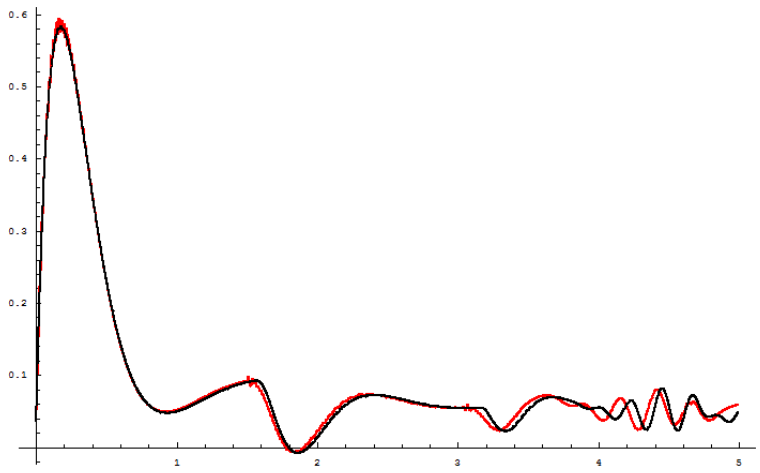

Figure 5.6: Thin Shell. $\dot{w}$ comparison in Head

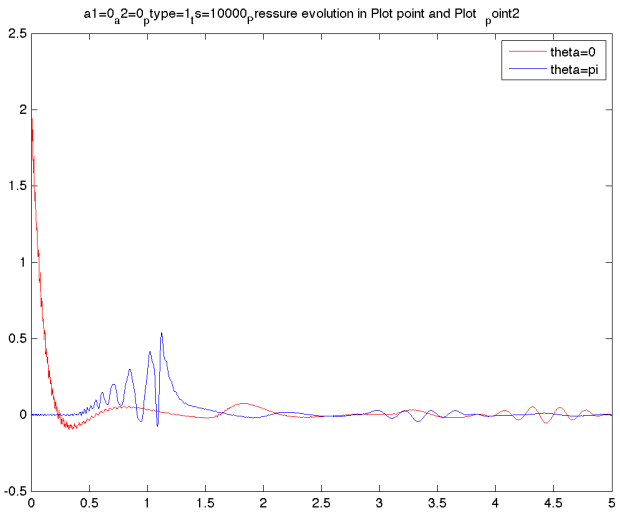

Figure 5.7: Thin Shell. Total pressure in Head and Tail

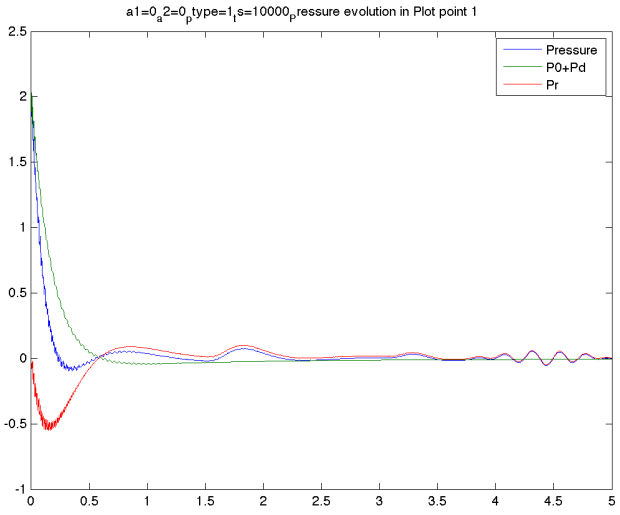

Figure 5.8: Thin Shell. Pressure decomposition in Head

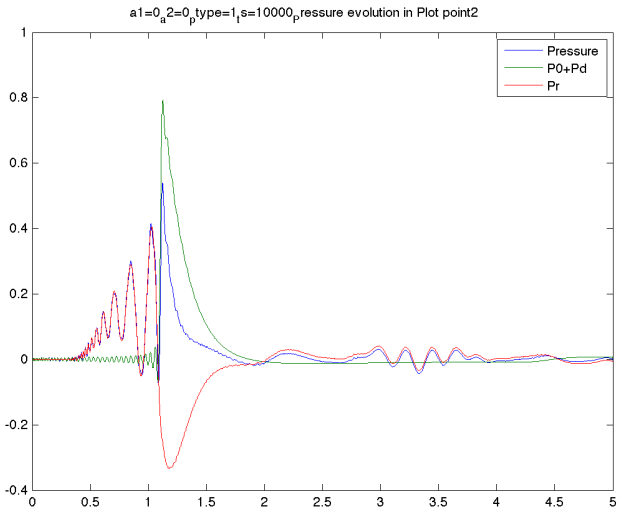

Figure 5.9: Thin Shell. Pressure decomposition in Tail

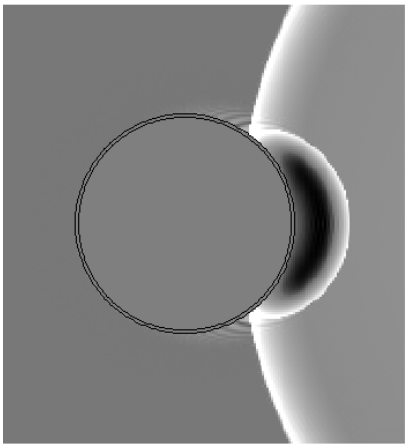

(a) Thin Shell. Acoustic field $\hat{t} = 0.5$

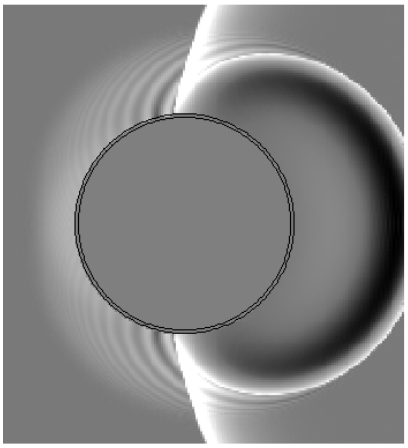

(b) Thin Shell. Acoustic field $\hat{t} = 1.2$

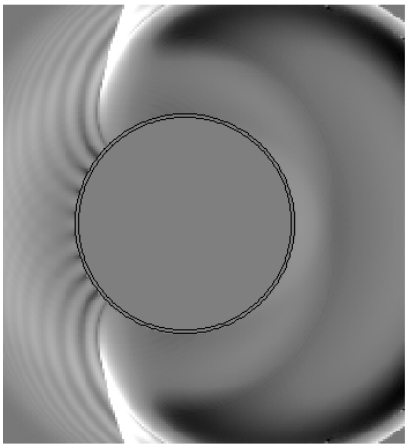

(c) Thin Shell. Acoustic field $\hat{t} = 1.9$

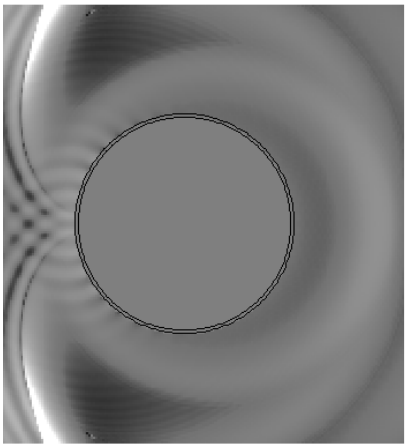

(d) Thin Shell. Acoustic field $\hat{t} = 2.6$

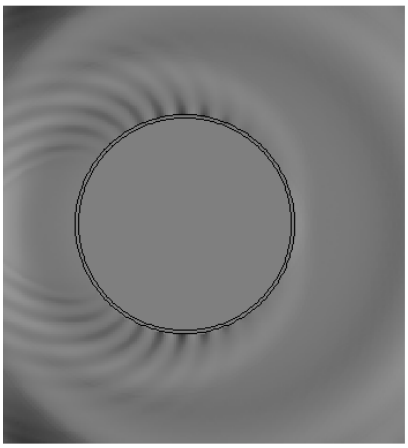

(e) Thin Shell. Acoustic field $\hat{t} = 3.3$

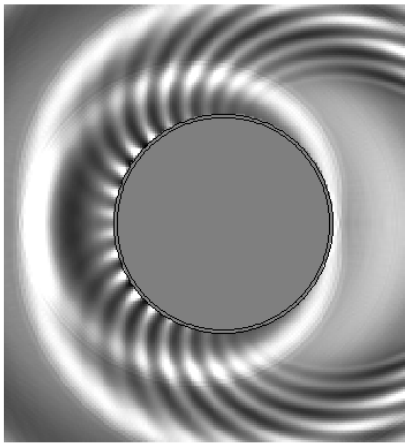

(f) Thin Shell. Acoustic field $\hat{t} = 4.0$

Figure 5.10: Thin Shell. Acoustic field

5.2 Heavy attached masses

As a second example, we have run a simulation using a the same thin evacuated shell made of steel of the previous simulation but we have added two heavy masses made of lead.

Geometry		
r_0	$1.00\,m$	Outer radius
h_0	$0.03\,m$	Thickness
α	$\pm 3\pi/4$	Starting angle of the added masses
h	$0.15\,m$	Added masses height
w	9°	Added masses angular widht
Materials		
E_s	$4.5895 \cdot 10^{11}\,Pa$	Young Modulus steel
ν_s	0.30	Poisson Coefficient steel
c_{s_s}	$7,990\,m/s$	Sound speed in solid steel
ρ_s	$7,900\,kg/m^3$	Density steel
E_l	$16 \cdot 10^9\,Pa$	Young Modulus lead
ν_l	0.25	Poisson Coefficient lead
c_{s_l}	$1,226.78\,m/s$	Sound speed in solid lead
ρ_l	$11,340\,kg/m^3$	Density lead

On the next figures we can see first the geometry and the used mesh (figures 5.11 and 5.11). Then we have plotted the displacement in radial direction w both in Head and Tail (figure 5.13) and also its velocities $\dot{w}$ (figure 5.14). In figure 5.15 we can see the total pressure evolution in Head and Tails, while in figures 5.16 and 5.17 we can see the contribution of the incident and the diffracted wave ($p_0 + p_d$) and the radiated wave (p_r) for both Head and Tail.

In figure 5.18 we can see the the reconstruction of the acoustic field for times $\hat{t} = 0.5$, $\hat{t} = 1.2$, $\hat{t} = 1.9$, $\hat{t} = 2.6$, $\hat{t} = 3.3$ and $\hat{t} = 4.0$. In this case, the result can be seen as the addition of the acoustic field for the thin shell plus the effect of the two attached masses. The attached masses act as fuming for the propagation of the shock inside the solid, but then, when the solid starts to vibrate, they act as a source of acoustic pulses in the fluid domain with low frequency.

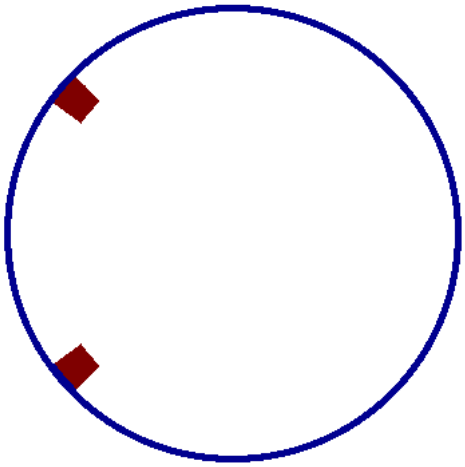

Figure 5.11: Heavy Masses. Geometry

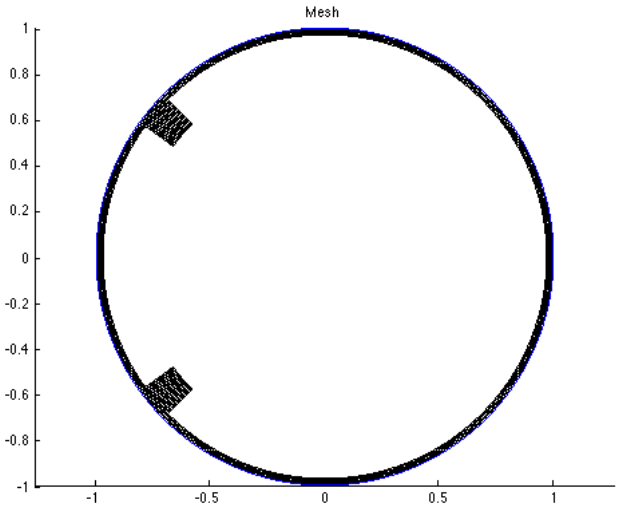

Figure 5.12: Heavy Masses. Mesh

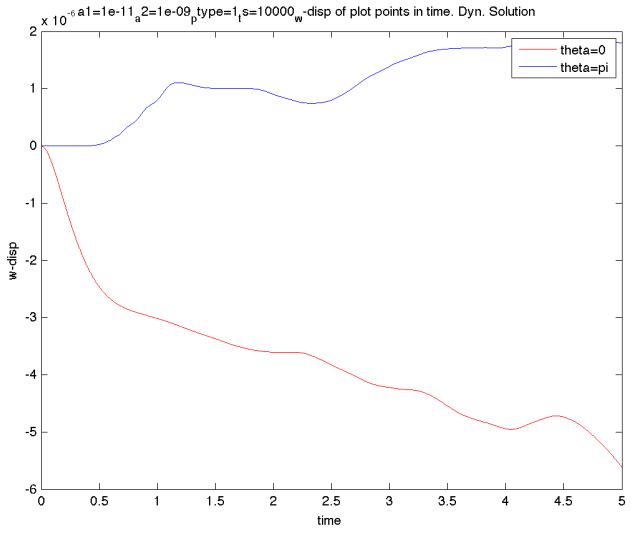

Figure 5.13: Heavy Masses. w in Head and Tail

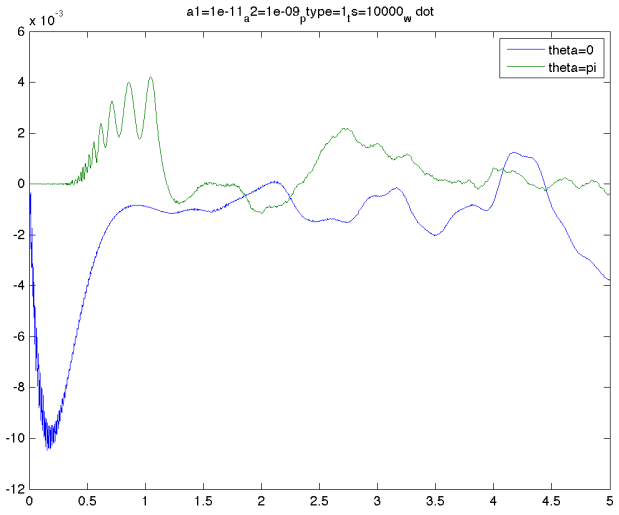

Figure 5.14: Heavy Masses. $\dot{w}$ in Head and Tail

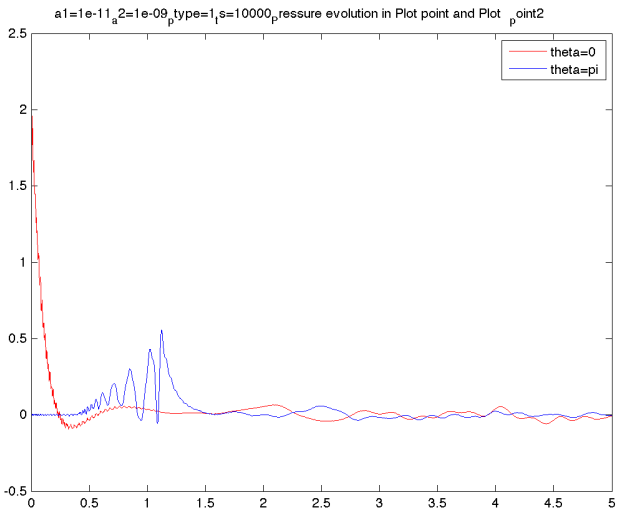

Figure 5.15: Heavy Masses. Total pressure in Head and Tail

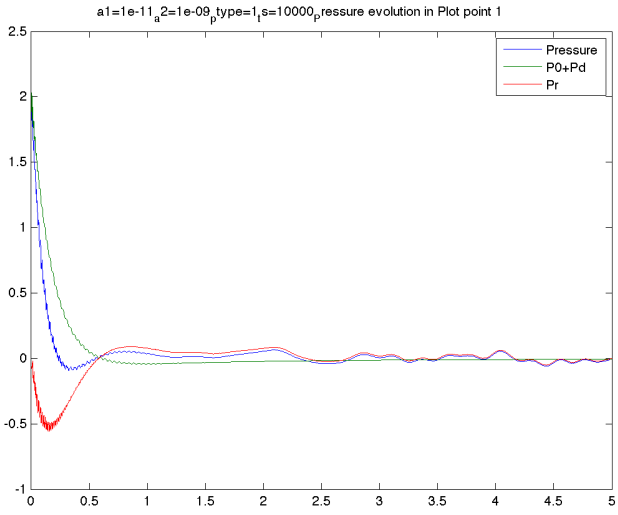

Figure 5.16: Heavy Masses. Pressure decomposition in Head

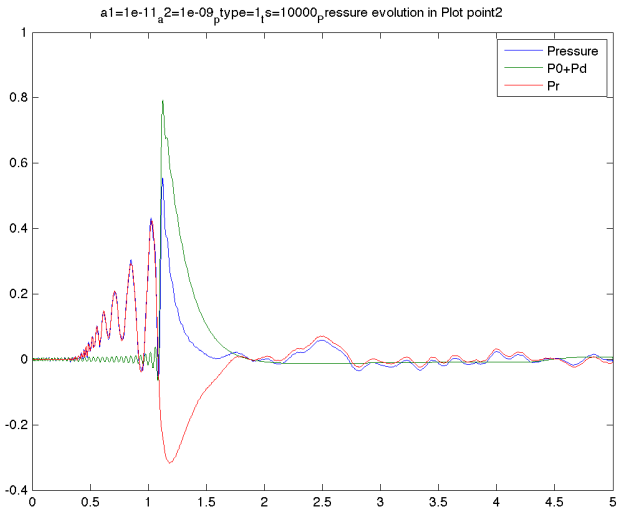

Figure 5.17: Heavy Masses. Pressure decomposition in Tail

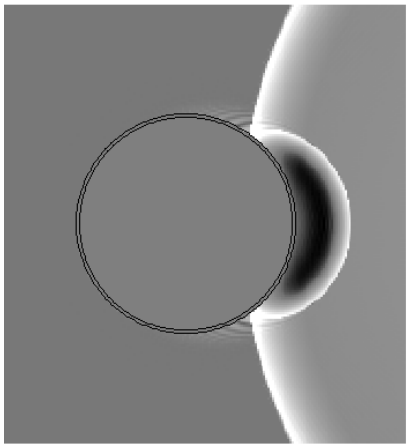

(a) Heavy Massess. Acoustic field $\hat{t} = 0.5$

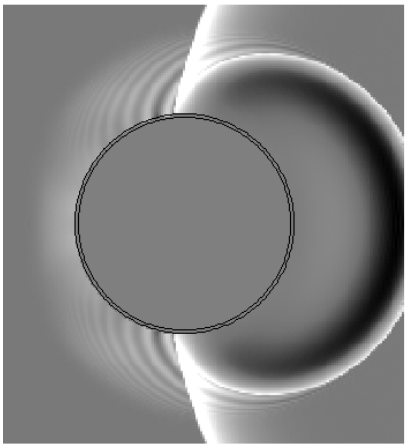

(b) Heavy Massess. Acoustic field $\hat{t} = 1.2$

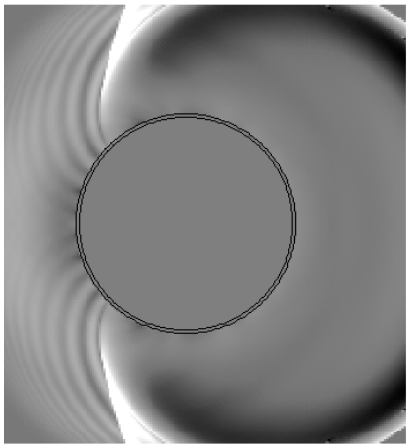

(c) Heavy Massess. Acoustic field $\hat{t} = 1.9$

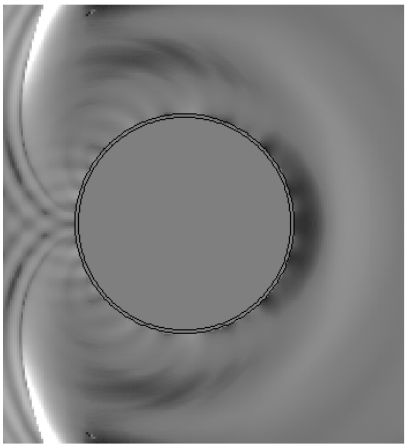

(d) Heavy Massess. Acoustic field $\hat{t} = 2.6$

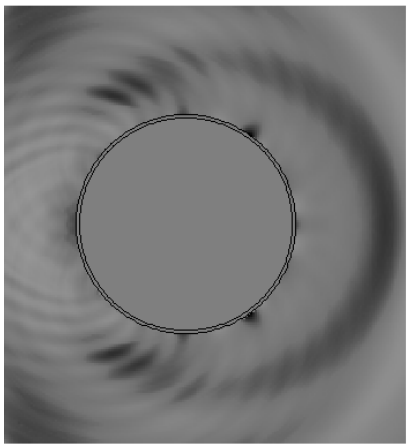

(e) Heavy Massess. Acoustic field $\hat{t} = 3.3$

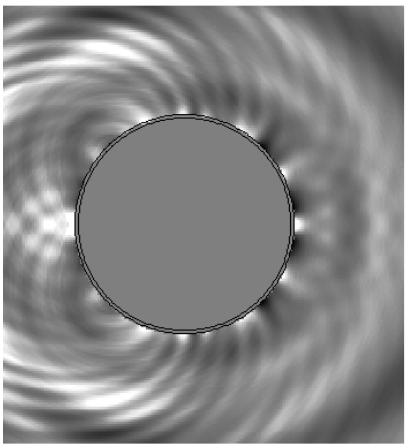

(f) Heavy Massess. Acoustic field $\hat{t} = 4.0$

Figure 5.18: Heavy Masses. Acoustic field

5.3 Light attached masses

Next example is adding 2 masses also but in this case they are much smaller and made of the same material. We can see in the problem description in the following table.

Geometry		
r_0	$1.00\,m$	Outer radius
h_0	$0.03\,m$	Thickness
α	$\pm\pi/4$	Starting angle of the added masses
h	$0.03\,m$	Added masses height
w	$1.8°$	Added masses angular width
Materials		
E	$4.5895 \cdot 10^{11}\,Pa$	Young Modulus
ν	0.30	Poisson Coefficient
c_s	$7,990\,m/s$	Sound speed in solid
ρ	$7,900\,kg/m^3$	Density

On the next figures we can see first the geometry and the used mesh (figures 5.19 and 5.19). Then we have plotted the displacement in radial direction w both in Head and Tail (figure 5.21) and also its velocities $\dot{w}$ (figure 5.22). In figure 5.23 we can see the total pressure evolution in Head and Tails, while in figures 5.24 and 5.25 we can see the contribution of the incident and the diffracted wave ($p_0 + p_d$) and the radiated wave (p_r) for both Head and Tail.

In figure 5.26 we can see the the reconstruction of the acoustic field for times $\hat{t} = 0.5$, $\hat{t} = 1.2$, $\hat{t} = 1.9$, $\hat{t} = 2.6$, $\hat{t} = 3.3$ and $\hat{t} = 4.0$. As in the previous example of the heavy masses, seen in section 5.2, we can see the acoustic field as the superposition of the one generated by the shell plus the generated by the light masses. We can see the effect is very similar to the one produced by the heavy masses, but now the frequency is higher.

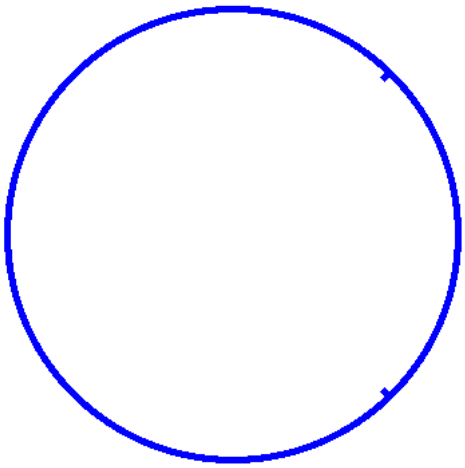

Figure 5.19: Light Masses. Geometry

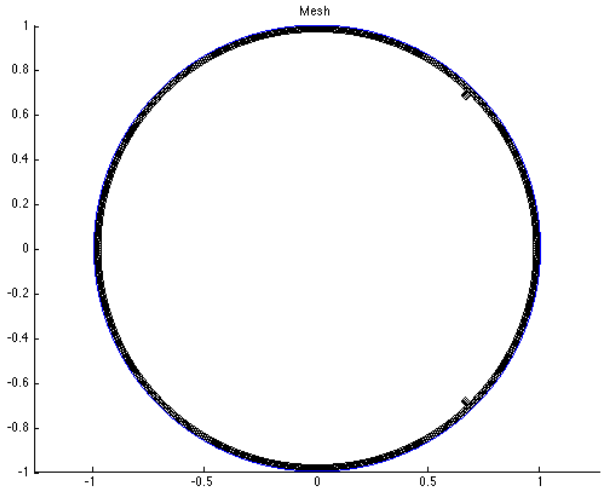

Figure 5.20: Light Masses. Mesh

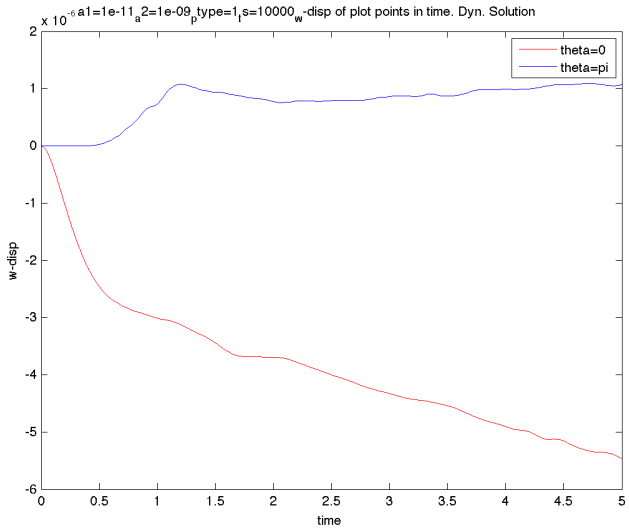

Figure 5.21: Light Masses. w in Head and Tail

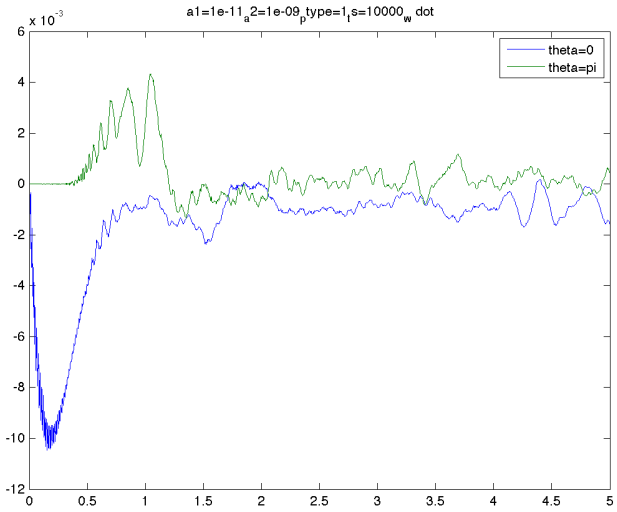

Figure 5.22: Light Masses. $\dot{w}$ in Head and Tail

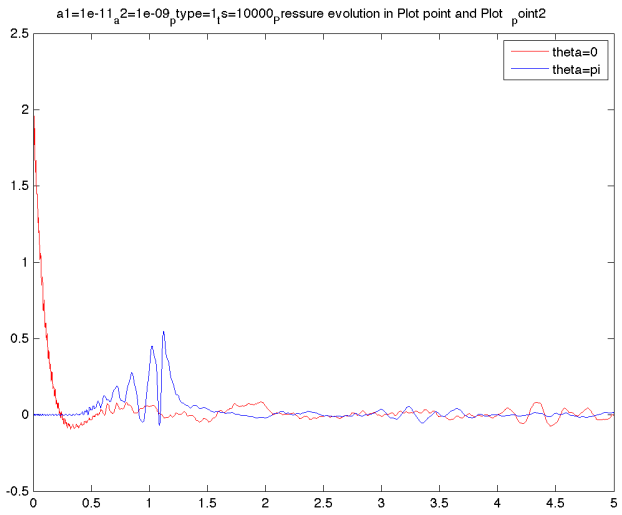

Figure 5.23: Light Masses. Total pressure in Head and Tail

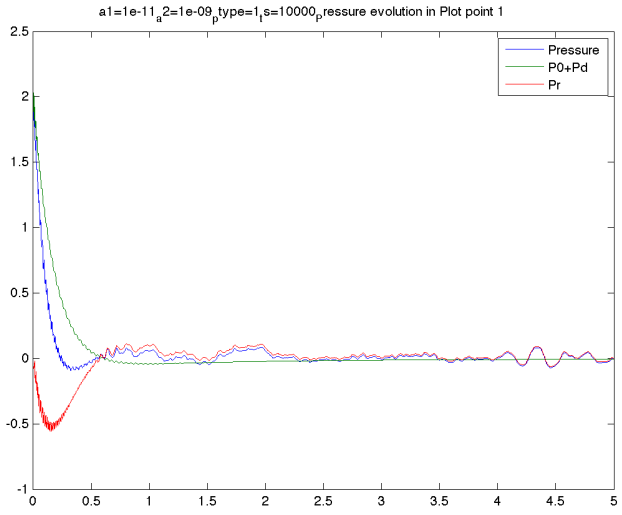

Figure 5.24: Light Masses. Pressure decomposition in Head

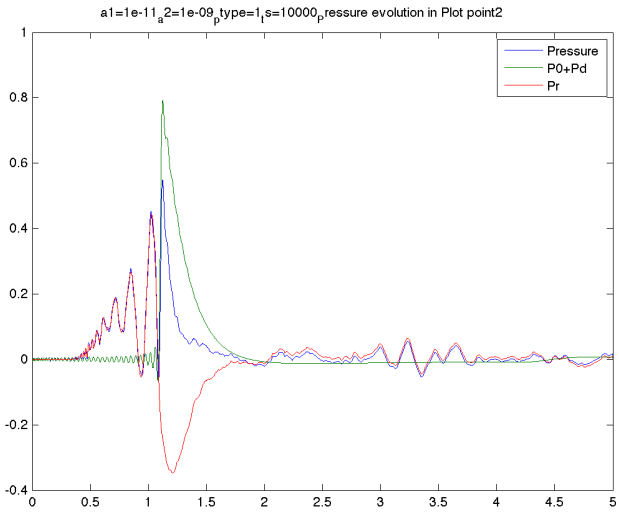

Figure 5.25: Light Masses. Pressure decomposition in Tail

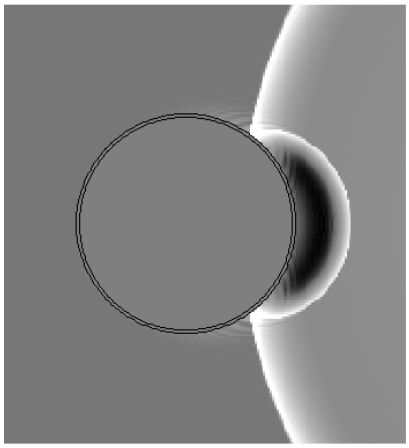

(a) Light Masses. Acoustic field $\hat{t} = 0.5$

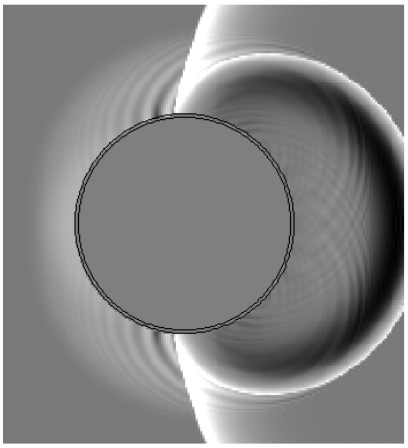

(b) Light Masses. Acoustic field $\hat{t} = 1.2$

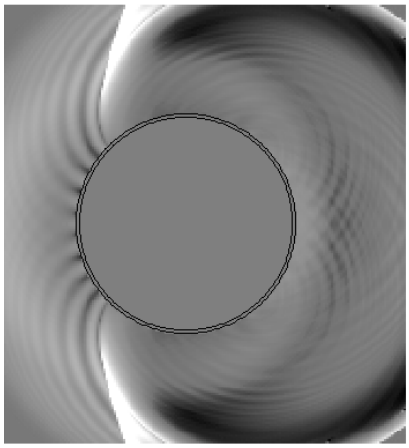

(c) Light Masses. Acoustic field $\hat{t} = 1.9$

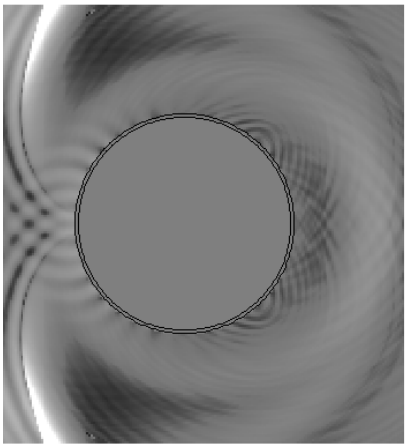

(d) Light Masses. Acoustic field $\hat{t} = 2.6$

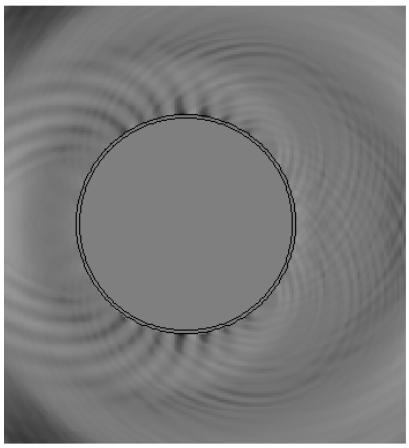

(e) Light Masses. Acoustic field $\hat{t} = 3.3$

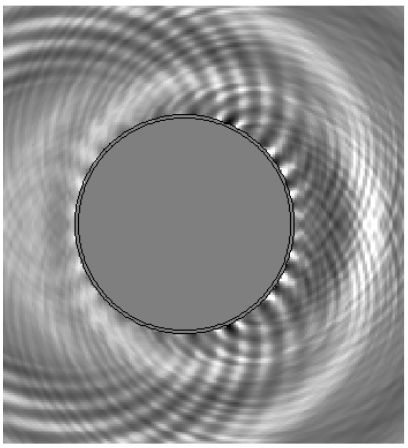

(f) Light Masses. Acoustic field $\hat{t} = 4.0$

Figure 5.26: Light Masses. Acoustic field

5.4 Reinforced structure

Now we have added a vertical reinforcement of the same material, placed in the oposite side the shockwave comes from. Here we can see the parameters that govern the problem.

Geometry		
r_0	$1.00\,m$	Outer radius
h_0	$0.03\,m$	Thickness
α	$\pm 3\pi/4$	Starting angle of the reinforcement
w	$0.0212\,m$	reinforcement width
Materials		
E	$4.5895 \cdot 10^{11}\,Pa$	Young Modulus
ν	0.30	Poisson Coefficient
c_s	$7,990\,m/s$	Sound speed in solid
ρ	$7,900\,kg/m^3$	Density

On the next figures we can see first the geometry and the used mesh (figures 5.27 and 5.27). Then we have plotted the displacement in radial direction w both in Head and Tail (figure 5.29) and also its velocities $\dot{w}$ (figure 5.30). In figure 5.31 we can see the total pressure evolution in Head and Tails, while in figures 5.32 and 5.33 we can see the contribution of the incident and the diffracted wave ($p_0 + p_d$) and the radiated wave (p_r) for both Head and Tail.

In figure 5.34 we can see the the reconstruction of the acoustic field for times $\hat{t} = 0.5$, $\hat{t} = 1.2$, $\hat{t} = 1.9$, $\hat{t} = 2.6$, $\hat{t} = 3.3$ and $\hat{t} = 4.0$. In this case, we can see a very similar effect to the one produced by he masses, but now the effect of the dumping is much more evident. The reinforcement also adds a new bifurcation for shockwave in the solid, so that it generates sort of an interference in the vibration of the shell creating a more blurred acoustic field.

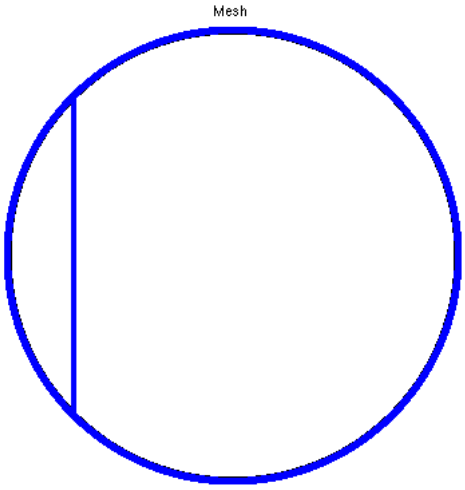

Figure 5.27: Reinforced Structure. Geometry

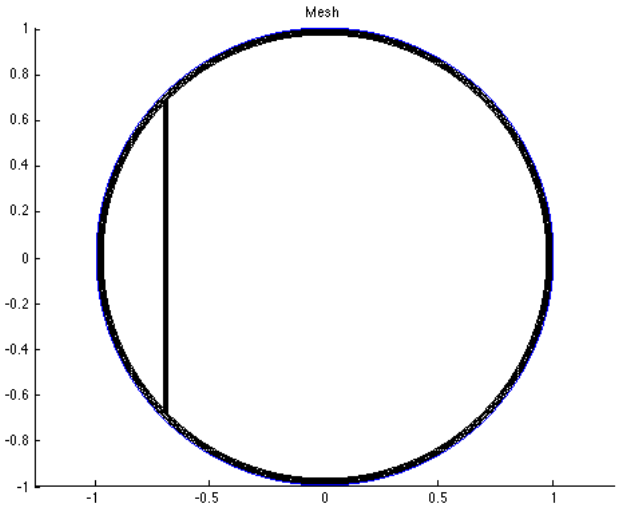

Figure 5.28: Reinforced Structure. Mesh

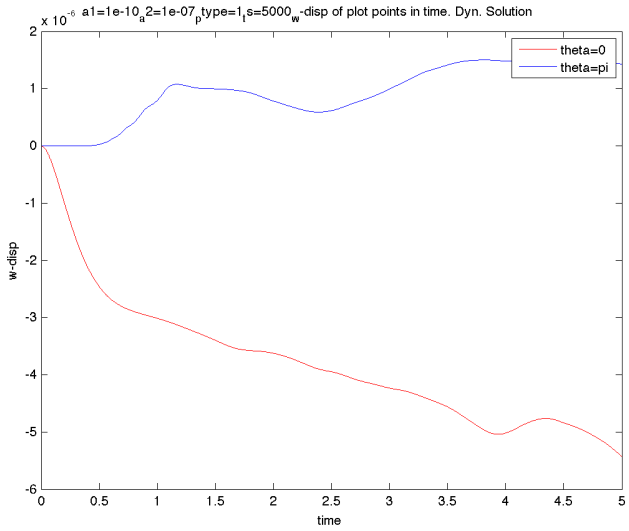

Figure 5.29: Reinforced Structure. w in Head and Tail

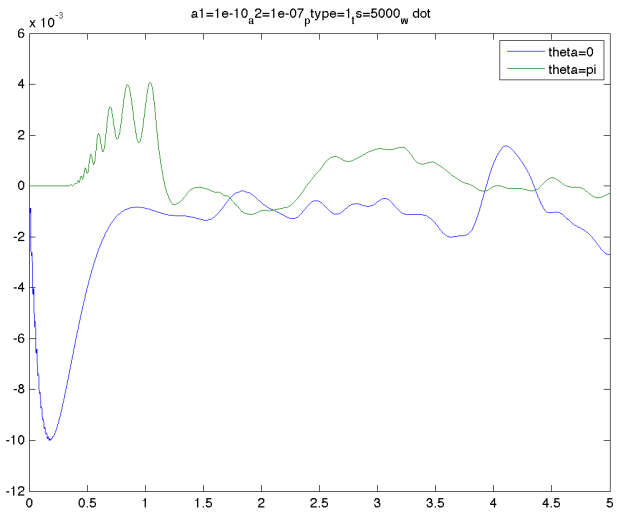

Figure 5.30: Reinforced Structure. $\dot{w}$ in Head and Tail

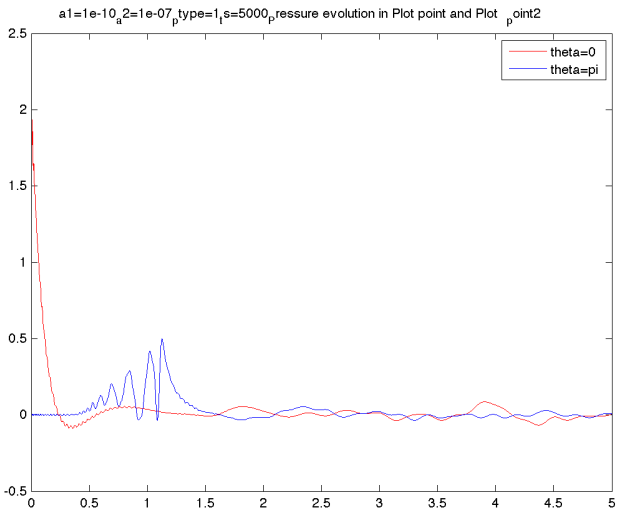

Figure 5.31: Reinforced Structure. Total pressure in Head and Tail

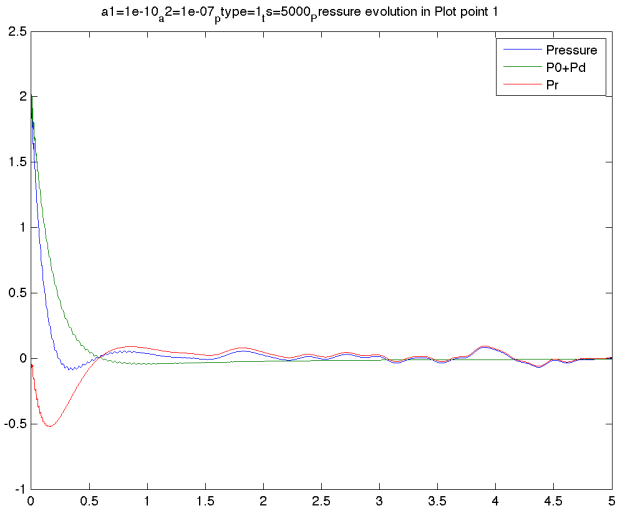

Figure 5.32: Reinforced Structure. Pressure decomposition in Head

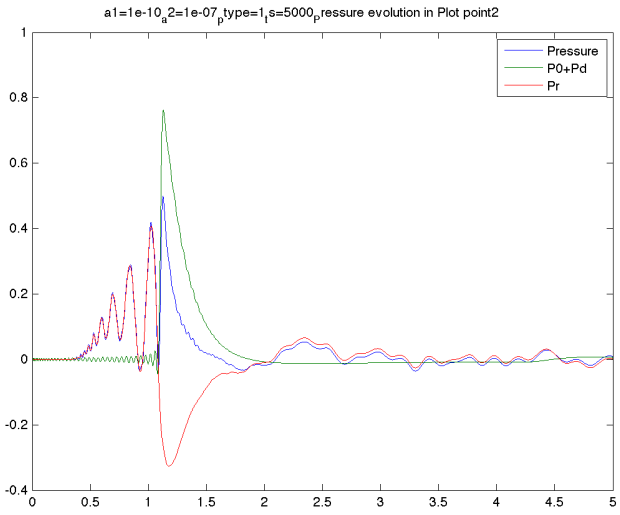

Figure 5.33: Reinforced Structure. Pressure decomposition in Tail

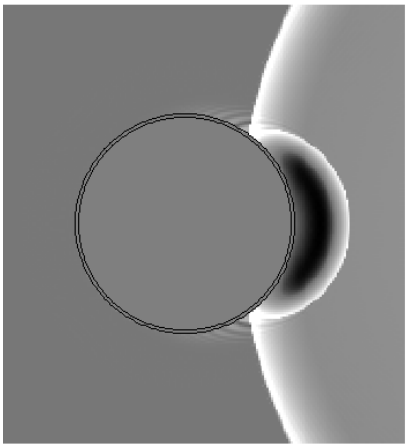

(a) Reinforced Structure. $\hat{t} = 0.5$

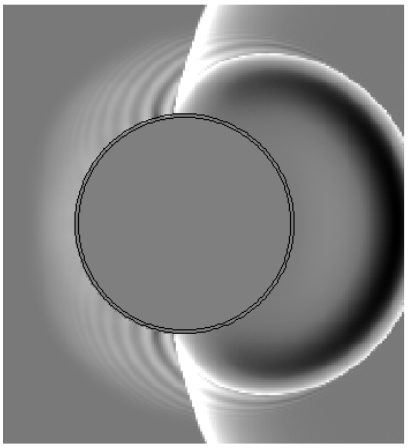

(b) Reinforced Structure. $\hat{t} = 1.2$

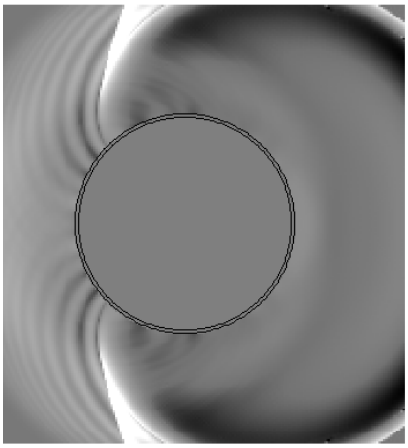

(c) Reinforced Structure. $\hat{t} = 1.9$

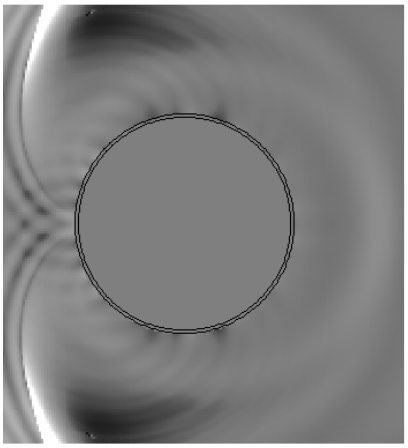

(d) Reinforced Structure. $\hat{t} = 2.6$

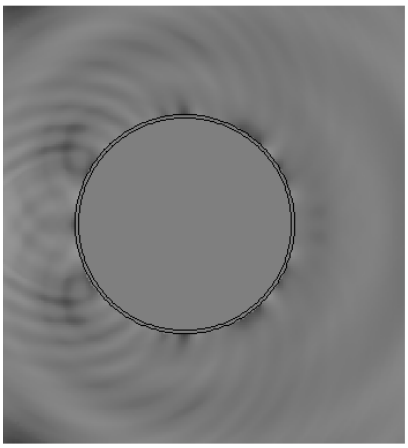

(e) Reinforced Structure. $\hat{t} = 3.3$

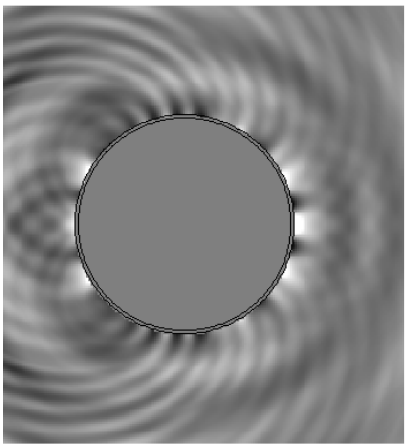

(f) Reinforced Structure. $\hat{t} = 4.0$

Figure 5.34: Reinforced Structure. Acoustic field

Appendix A

Notation

Variable	Meaning	Adimensional
c_f	Sound speed in the fluid	$\hat{c}_f = 1$
c_s	Sound speed in the solid	$\hat{c}_s = c_s c_f^{-1}$
E	Young Modulus (Related to c_s)	
I_n	Modified Bessel function of the first kind of order n	
I^x_{CP}	Transformation matrix from cartesian to polar. X direction	
I^y_{CP}	Transformation matrix from cartesian to polar. X direction	
I_{FS}	Transformation matrix from fluid to solid mesh	
I_{HV}	Transformation matrix from harmonics to mesh values	
I_{SF}	Transformation matrix from solid to fluid mesh	
I_{VH}	Transformation matrix from mesh values to harmonics	
K_n	Modified Bessel function of the second kind of order n	
K	F.E.M. Stiffness Matrix	
$K*$	F.E.M. Neumark modified Stiffness Matrix	
M	F.E.M. Mass matrix	
p_α	Peak incident pressure	$\hat{p}_\alpha = p_\alpha \rho_f^{-1} c_f^{-2}$
p_0	Incident pressure	$\hat{p}_0 = p_0 \rho_f^{-1} c_f^{-2}$
p_d	Difraction pressure	$\hat{p}_d = p_d \rho_f^{-1} c_f^{-2}$
p_r	Radiated pressure	$\hat{p}_r = p_r \rho_f^{-1} c_f^{-2}$
p	Total pressure on the fluid	$\hat{p} = p \rho_f^{-1} c_f^{-2}$
r	Radial coordinate of the polar system	$\hat{r} = r r_0^{-1}$

Variable	Meaning	Adimensional
r_0	Outer radius of the body	$\hat{r}_0 = 1$
R_0	Radial distance to the source of the incident wave	$\hat{R}_0 = R_0 r_0^{-1}$
t	Time	$\hat{t} = t c_f r_0^{-1}$
u	Horizontal displacement	$\hat{u} = u r_0^{-1}$
U	F.E.M. Nodal displacement vector	
v	Vertical displacement	$\hat{v} = v r_0^{-1}$
w	Radial displacement	$\hat{w} = w r_0^{-1}$
ϵ	Strain tensor	
θ	Angular coordinate of the polar coordinate system	
ν	Poisson ratio	
ξ	Volume response function	
ρ_f	Density of the fluid	$\hat{\rho}_f = 1$
ρ_s	Density of the solid	$\hat{\rho}_s = \rho_s \rho_f^{-1}$
ϕ	Fluid velocity potential	$\hat{\phi} = \phi c_f^{-1} r_0^{-1}$
ϕ_0	Fluid velocity potential due to the incident wave	$\hat{\phi}_0 = \phi_0 c_f^{-1} r_0^{-1}$
ϕ_d	Fluid velocity potential due to the diffracted wave	$\hat{\phi}_d = \phi_d c_f^{-1} r_0^{-1}$
ϕ_r	Fluid velocity potential due to the radiated wave	$\hat{\phi}_r = \phi_r c_f^{-1} r_0^{-1}$
ψ	Surface response function	

Table A.1: Notation

Harmonic series term: We denote with a subscript the n-th term of the Fourier serie as $(\cdot)_n$, so that they will be $(\cdot)_n \sin(n\theta)$ and $(\cdot)_n \cos(n\theta)$.

Matrix notation: We denote with two subscript A_{ij} the term in the i-th file and j-th column.

Laplace transform: we use the capital letter of a small letter variable to denote the Laplace transform of the variable.

Other used notations are introduced in the text.

Bibliography

Iakovlev, S. (2002). Interaction of a spherical shock wave and a submerged fluid-filled circular cylindrical shell. *Journal of sound and vibration 255*(4), 615–633.

Iakovlev, S. (2004). Influence of a rigid coaxial core on the stress–strain state of a submerged fluid-filled circular cylindrical shell subjected to a shock wave. *Journal of Fluids and Structures 19*(7), 957–984.

Iakovlev, S. (2006). External shock loading on a submerged fluid-filled cylindrical shell. *Journal of Fluids and Structures 22*(8), 997–1028.

Iakovlev, S. (2007). Submerged fluid-filled cylindrical shell subjected to a shock wave: fluid–structure interaction effects. *Journal of fluids and structures 23*(1), 117–142.

Iakovlev, S. (2008a). Interaction between a submerged evacuated cylindrical shell and a shock wave—part i: Diffraction–radiation analysis. *Journal of Fluids and Structures 24*(7), 1077–1097.

Iakovlev, S. (2008b). Interaction between a submerged evacuated cylindrical shell and a shock wave—part ii: Numerical aspects of the solution. *Journal of Fluids and Structures 24*(7), 1098–1119.

Iakovlev, S. (2009). Interaction between an external shock wave and a cylindrical shell filled with and submerged into different fluids. *Journal of Sound and vibration 322*(1), 401–437.

Iakovlev, S., G. Dooley, K. Williston, and J. Gaudet (2011). Evolution of the reflection and focusing patterns and stress states in two-fluid cylindrical shell systems subjected to an external shock wave. *Journal of Sound and Vibration 330*(25), 6254–6276.

Iakovlev, S., M. Mitchell, and G. Dooley (2011). Modeling two-fluid response of thin elastic shells. *International Journal for Numerical Methods in Fluids 65*(11-12), 1389–1406.

Iakovlev, S., H. Santos, K. Williston, R. Murray, and M. Mitchell (2013). Non-stationary radiation by a cylindrical shell: Numerical modeling using the reissner–mindlin theory. *Journal of Fluids and Structures 36*, 50–69.

Oñate, E. (2004). *Cálculo de Estrucutras por el Método de los Elementos Finitos*. Universitat Politècnica de Cataluna.

Zienkiewicz, O. and R.L.Taylor (1994a). *El Método de los Elementos Finitos* (4 ed.), Volume 1. Mc.Graw-Hill.

Zienkiewicz, O. and R.L.Taylor (1994b). *El Método de los Elementos Finitos* (4 ed.), Volume 2. Mc.Graw-Hill.